Energy Conversion and Management 345 (2025) 120400

Contents lists available at ScienceDirect

Energy Conversion and Management

journal homepage: www.elsevier.com/locate/enconman

A novel energy management system based on move-blocking based predictive control for use in microgrid control

Pajares A.[a,*], Vivas F.J.[b], Blasco X.[a], Herrero J.M.[a], Segura F.[b], Andújar J.M.[b]

[a] Instituto Universitario de Automática e Informática Industrial, Universitat Politècnica de València, Valencia, Spain
[b] Research Centre on Technology, Energy and Sustainability (CITES), University of Huelva, Spain

ARTICLE INFO

Keywords:
Move-blocking
Optimal control
Model predictive controller
Energy management system
Renewable microgrids
Hydrogen-based store system

ABSTRACT

The increasing complexity of renewable-based microgrids demands advanced Energy Management Systems (EMS) capable of efficiently managing multi-time scale dynamics. Conventional Model Predictive Control (MPC) based EMS often rely on complex hierarchical structures with problematic weighting factors, which can cause undesirable effects, leading to suboptimal performance. This work proposes and validates an innovative single-layer EMS that leverages a move-blocking strategy. The key novelty lies in embedding long-term economic objectives and short-term physical constraints into a unified optimisation problem, eliminating the need for hierarchical layers and manual weight tuning. The performance of the proposed EMS was benchmarked against a conventional bilevel hierarchical EMS and an optimal reference case. The results demonstrate significant quantitative and qualitative improvements. Our approach reduces total operating costs by over 8%. This saving is composed of several key factors: a 13 % decrease in degradation-related costs attributable to more stable management of the hydrogen system, a reduction in fixed operating costs by minimising the usage time of the hydrogen systems, and a 7 % reduction in variable energy costs. Computationally, the strategy is highly efficient, reducing computation time by 99 % compared to the optimal case and confirming its real-time feasibility. Furthermore, it ensures more stable operation of the hydrogen system and increases system autonomy. These findings position the proposed move-blocking MPC framework as a scalable, robust, and computationally efficient solution for intelligent energy management in next-generation microgrids.

1. Introduction

The global transition toward sustainable energy has accelerated the development of microgrids as essential platforms for the integration of renewable energy sources within distributed power systems [1,2]. These systems enable the seamless incorporation of clean energy generation with advanced energy management strategies, thereby enhancing the resilience, efficiency, and sustainability of modern electrical grids [3,4]. Of particular importance is the integration of hybrid energy storage systems (HESS), comprising battery stack storage (BSS) and hydrogen-based storage systems (HBSS), which significantly augments both energy capacity and dynamic responsiveness [5,6]. However, these technological advancements also introduce substantial challenges related to the control and optimisation of systems operating across multiple time scales. Traditional EMS often struggle to simultaneously manage fast-timescale power balancing (on the order of seconds), mid-timescale economic dispatch (ranging from minutes to hours), and long-term asset degradation mitigation [7,8].

In the early stages of microgrid development, EMS implementations primarily relied on heuristic or rule-based strategies [9,10]. While computationally efficient, these approaches lacked the ability to ensure economic optimality or rigorously enforce complex operational constraints [11,12]. Consequently, MPC emerged as a promising alternative, owing to its suitability for constrained multivariable systems and its capacity for predictive optimisation, disturbance rejection, and multi-objective control [13–16]. Several studies have reported that applying MPC to microgrids with HESS yields a 12–15 % reduction in operating costs compared to heuristic-based methods [17,18].

Despite these advantages, conventional MPC frameworks face significant challenges when applied to complex microgrid architectures characterized by multiple constraints and composite objective functions. These challenges frequently render real-time implementation computationally infeasible [19,20]. As a result, recent efforts have focused developing advanced MPC-based methods that maintain performance while enhancing computationally efficiency, thereby addressing the

* Corresponding author.
E-mail address: alpafer1@upv.es (A. Pajares).

https://doi.org/10.1016/j.enconman.2025.120400
Received 18 June 2025; Received in revised form 2 August 2025; Accepted 17 August 2025
Available online 25 August 2025

Nomenclature

Acronyms

BoP	Balance of plant
BSS	Battery-based storage system
EMS	Energy management system
ESS	Energy storage system
HBSS	Hydrogen-based storage system
HESS	Hybrid energy storage system
HL	High-level
LL	Low-level
MB	Move-blocking
MEG	Main electrical grid
MPC	Model-based predictive control
PH	Prediction horizon
SOC	State of charge

Symbols

C_i^{var}	Variable cost of HESS and MEG ($i = \{ch_{bat}, dis_{bat}, ch_{H2}, dis_{H2}, grid_p, grid_s\}$) (€/Wh)
C_i^{fix}	Fixed cost of HESS and MEG ($i = \{ch_{bat}, dis_{bat}, ch_{H2}, dis_{H2}, grid_p, grid_s\}$) (€/h)
C_i^{start}	Start cost of HESS and MEG ($i = \{ch_{bat}, dis_{bat}, ch_{H2}, dis_{H2}, grid_p, grid_s\}$)(€)
C_i^{degr}	Degradation cost of HESS and MEG ($i = \{ch_{bat}, dis_{bat}, ch_{H2}, dis_{H2}, grid_p, grid_s\}$)(€/W^2)
CN_j	Energy capacity of element ($j = \{bat, H2\}$) (Wh)
ESS_j	Energy storage system ($j = \{bat, H2\}$)
ΔP_i	Power variation of HESS and MEG ($i = \{ch_{bat}, dis_{bat}, ch_{H2}, dis_{H2}, grid_p, grid_s\}$)(W)
δP_i	Increment power without on and/or off process ($i = \{ch_{bat}, dis_{bat}, ch_{H2}, dis_{H2}, grid_p, grid_s\}$)(W)
η_{ch/dis_j}	Charge/discharge efficiency related to element ESS_j ($j = \{bat, H2\}$) (%)
$\overline{H}/\underline{H}$	Maximum and minimum value of variable H (H $= \{x, P_i, \Delta P_i\}$)
K_{Pch}/K_{Pdis}	Coef. to BSS related to BSS charge/disc. power (V/W)
K_{SOC}	Coef. to BSS related to SOC (V/%)
$K_{V_{BUS}}$	Coef. to BSS related to V_{BUS}
$Loss$	Total losses of the microgrid (W)
$Loss_i$	Variable losses depending on the power of HESS and MEG ($i = \{ch_{bat}, dis_{bat}, ch_{H2}, dis_{H2}, grid_p, grid_s\}$) (W)
$Loss_i^{BoP}$	Balance of plant of HESS and MEG ($i = \{ch_{bat}, dis_{bat}, ch_{H2}, dis_{H2}, grid_p, grid_s\}$) (W)
$\omega_{\delta P_i}$	Weight to penalise power variation
ω_{P_i}	Weight to penalise power tracking error
ω_{Start_i}	Weight to penalise the number of start-ups
ω_{SOC_j}	Weight to penalise SOC tracking error
P_i	HESS and MEG power ($i = \{ch_{bat}, dis_{bat}, ch_{H2}, dis_{H2}, grid_p, grid_s\}$) (W)
P_{EV}	Electric vehicle power (W)
P_{Load}	Load power consumed from the microgrid (W)
P_{HA}	House appliance power (W)
P_{HVAC}	Heat., vent., and air cond. power (W)
P_i^{ref}	HESS and MEG reference power ($i = \{ch_{bat}, dis_{bat}, ch_{H2}, dis_{H2}, grid_p, grid_s\}$) (W)
$PH_{HL/LL}$	Prediction horizon of HL/LL (h)
P_{PV}	Renewable power injected by the microgrid (W)
r_{ch/dis_j}	Charge/discharge ratio related to element ESS_j ($j = \{bat, H2\}$) (%/W)
SOC_j	State of charge ($j = \{bat, H2\}$) (%)
SOC_j^{ref}	Reference state of charge ($j = \{bat, H2\}$) (%)
$Start_i$	Start of HESS and MEG ($i = \{ch_{bat}, dis_{bat}, ch_{H2}, dis_{H2}, grid_p, grid_s\}$) (binary)
T_S	Sample time (h)
$T_{SHL/LL}$	Sample time HL/LL (h)
V_{BUS}	DC bus (and BSS) voltage (V)
WT_i	Working time of HESS and MEG ($i = \{ch_{bat}, dis_{bat}, ch_{H2}, dis_{H2}, grid_p, grid_s\}$) (binary)
$x(k)$	State variable (SOC, LOH, V_{BUS})
v_k	Independent term related to V_{BUS} model (V)

intrinsic multi-time scale control challenges [21,22]. Among these, hierarchical architectures employing multi-level (typically bi-level) MPC have emerged as a widely adopted solution within the literature [13,23,24]. In such framework, a high-level MPC controller (HL-MPC) manages long-term economic dispatch over extended prediction horizons (PH), while a low-level MPC controller (LL-MPC) ensures rapid reference tracking and system stability [16,25,26].

The effectiveness of hierarchical MPC approaches have been demonstrated across diverse microgrid configurations. For instance, [27] and [28] present a hierarchical MPC scheme where a HL controller optimises long-term economic dispatch considering hydrogen production and battery states, while a LL controller manages power balancing. Expanding on this concept, in [29] a distributed hierarchical MPC is proposed using multi-agent framework in which each agent operates a self-triggered MPC, allowing for scalable and decentralized energy management. Aiming to alleviate computational complexity, [30] introduces a hierarchical coordination scheme that eschews explicit predictive models, enabling multi-time-scale planning across BSS and HBSS with reduced computational overhead. Furthermore, [31] explores hierarchical MPC for coordinating electric and hydrogen energy flows in integrated charging stations, achieving optimisation of operational costs and emissions over multiple time scales.

Despite their widespread use, hierarchical MPC strategies exhibit several critical limitations. These include: (1) the sensitivity of LL-MPC performance empirically-tuned weighting factors; (2) economic inefficiencies arising from strict adherence to HL-MPC references in volatile pricing scenarios; and (3) computational bottlenecks in large-scale HESS deployments [11,22,32]. These limitations have stimulated the investigation of alternative MPC formulations that maintain real-time feasibility while enhancing economic performance. Two notable approaches in this regard are Move-Blocking MPC (MB-MPC) [33,34] and Variable Horizon MPC (VH-MPC) [35,36].

MB-MPC addresses computational complexity by segmenting future control actions into fixed intervals during which control inputs remain constant. This reduction in degrees of freedom streamlines the optimisation without altering the underlying system dynamics [37,38]. As a result, MB-MPC retains the predictive benefits of classical MPC while substantially reducing computational demands. Applications across various domains have validated its effectiveness: for instance, in electric vehicle energy management, [39] MB-MPC has enabled faster online computations without compromising performance; in campus-wide thermal systems[40], it has reduced energy costs and maintained user comfort; and in DC microgrids [41,42], it has enhanced voltage control efficiency and minimised switching losses in multi-converter systems.

However, for systems exhibiting both fast and slow dynamics, such as microgrids with HESS, fixed blocking intervals may reduce control flexibility, potentially resulting in suboptimal responses, constraint violations, or even infeasibility [43,44]. The successful application of MB-MPC in such systems necessitates a nuanced understanding of the plant dynamics to appropriately tailor the blocking structure [34,45].

In parallel, VH-MPC offers an alternative strategy by dynamically adjusting the prediction horizon during runtime while maintaining a fixed sampling interval. This flexibility allows for an adaptive trade-off between computational effort and forecast depth [46,47]. The method has proven effective in various fields: in autonomous navigation [35,48], VH-MPC adapts trajectory control to environmental uncertainty; in aerospace [46,49], it enables mission-phase-aware planning; and in battery thermal-electrical control for EVs [50], it enhances thermal regulation and longevity. In power electronics, [51] shows VH-MPC improves real-time feasibility for inverter control. Nonetheless, when applied to microgrid EMS, VH-MPC may compromise long-term economic optimality, particularly when reduced horizons fail to capture delayed effects such as storage degradation or dynamic energy pricing.

Taken together, the demonstrated advantages of MB-MPC and VH-MPC across a broad range of engineering applications underscore their untapped potential in microgrid EMS design, especially for systems incorporating HESS. This significant gap in the literature highlights a compelling opportunity for further research aimed at tailoring these advanced MPC formulations to the specific control demands and operational constraints of next-generation hybrid microgrids.

To address the identified research gaps, this paper proposes a novel, high-performance EMS founded on a computationally efficient MPC framework, specially designed for renewable microgrids with HESS. The proposed solution incorporates an advanced MB-MPC strategy that synergistically combines short receding horizons with a long shrinking prediction horizon. This enables holistic and scalable management of multi-time scale dynamics within a unified, single-layer control architecture.

A central innovation of this approach lies in its MPC formulation, which effectively balances high-resolution control of fast system dynamics with the long-term optimisation of slower processes. The short receding horizon is employed to track high-frequency events, such as rapid fluctuations in generation and load, and the internal dynamics of the BESS, using variable and fine sampling intervals. Simultaneously, the long shrinking horizon captures slower temporal dynamics, including energy trading and interactions with the day-ahead energy market, by applying coarser time steps and progressively contracting the prediction horizon at each iteration.

A key advantage of this control structure is the adoption of an economic objective function, which obviates the need for empirically-tuned weighting factors traditionally required in MPC schemes. This design choice not only simplifies the controller configuration process but also enhances robustness and performance consistency by avoiding suboptimal outcomes resulting from poorly calibrated weightings.

Thus, the main contributions of the paper can be summarised as follows:

- Development of a computationally efficient EMS based on an economic MPC framework that integrates move-blocking and shrinking horizon concepts, tailored specifically for renewable microgrids with fully integrated HESS.
- Introduction of a unified, single-level control architecture, which eliminates the need for hierarchical control structures. This simplification facilitates real-time implementation, reduces design complexity, and enables the direct modelling of critical interdependencies between temporal dynamics, thereby enhancing control consistency and effectiveness.
- Implementation of an economic optimisation criterion, replacing the conventional weighted-sum objective functions. This avoids manual tuning of weighting coefficients, thereby improving the reliability, transparency, and efficiency of controller programming.
- Quantitative evaluation of the trade-off between computational efficiency and optimality, through a comparative analysis involving the proposed MB-MPC approach, a conventional two-level hierarchical MPC EMS, and the theoretical optimal solution. The two-level MPC was selected as the reference benchmark due to its demonstrated efficacy and widespread adoption in the literature. Other approaches, such as Dynamic Programming and Variable-Horizon MPC, were excluded from the comparison on the grounds of limited practical feasibility and applicability to real-time EMS design.

The remainder of the article is structured as follows: Section 2 details the architecture and the renewable microgrid model under consideration. Sections 3 and 4 present the general formulation of the MB-MPC-based EMS and the two-level hierarchical MPC-based EMS, respectively. In Section 5, the constraints and the common formulation of the optimisation problem for the different MPC approaches are detailed. Section 6 provides the results of the proposed controller, comparing and discussing its performance relative to reference controllers. Finally, the main conclusions are summarised in Section 7.

2. Renewable-Energy based microgrid

2.1. Microgrid architecture

The objective of this research is to develop a MB-MPC framework for the optimal management of renewable-based residential microgrids equipped with HESS. The proposed EMS is designed to enhance both technical and economic performance, as well as to improve computational efficiency, when compared to the conventional approaches commonly adopted in the scientific literature.

To ensure a fair comparison between different EMS approaches, their design, implementation, and validation must be conducted on a well-established and widely recognised microgrid architecture. Nevertheless, the proposed control framework and system configuration are adaptable to a variety of microgrid setups.

Among the various microgrid architectures extensively investigated in the literature, one of the most thoroughly analysed is the residential direct current (DC) microgrid incorporating a HESS [1,52]. This setup integrates a BSS, an HBSS, and a connection to the Main Electrical Grid (MEG). Given its prominence and relevance, this architecture has been adopted as the basis for the present study. The specific microgrid architecture is illustrated in Fig. 1.

In this configuration, the microgrid consists of four main subsystems: generation, demand, energy storage, and the MEG, all interconnected via a centralised DC bus.

For renewable energy generation, the microgrid employs a photovoltaic (PV) array with output power P_{PV}, which is interfaced with the DC bus through a dedicated power converter.

On the demand side, the total load is composed of three distinct end-use profiles: household appliances and lighting (P_{HA}), heating, ventilation, and air conditioning (HVAC) systems (P_{HVAC}), and electric vehicle (EV) charging (P_{EV}). Each of these components is connected to the DC bus via individual power converters, and the load demand is given by $P_{LOAD} = P_{HVAC} + P_{HA} + P_{EV}$.

The energy storage system adopts a hybrid architecture, combining two complementary technologies with differing response times and storage capacities. The BSS provides short- to medium-term energy storage (P_{bat}) and is directly coupled to the DC bus. It is responsible for mitigating real-time power imbalances between energy generation and consumption and for stabilising the DC bus voltage, particularly during abrupt fluctuations in generation or load demand. While the BSS supports voltage regulation, the EMS is tasked with managing the battery's charge and discharge cycles to ensure that voltage levels remain within a permissible bound.

Complementing the ESS, the HBSS is designed for long-term energy storage and manages the entire hydrogen energy cycle. This includes hydrogen production, storage, and reconversion to electricity. The HBSS comprises an electrolyser (with power input $P_{ch_{H2}}$), a hydrogen storage tank, and a fuel cell (with power output $P_{dis_{H2}}$), each connected to the DC

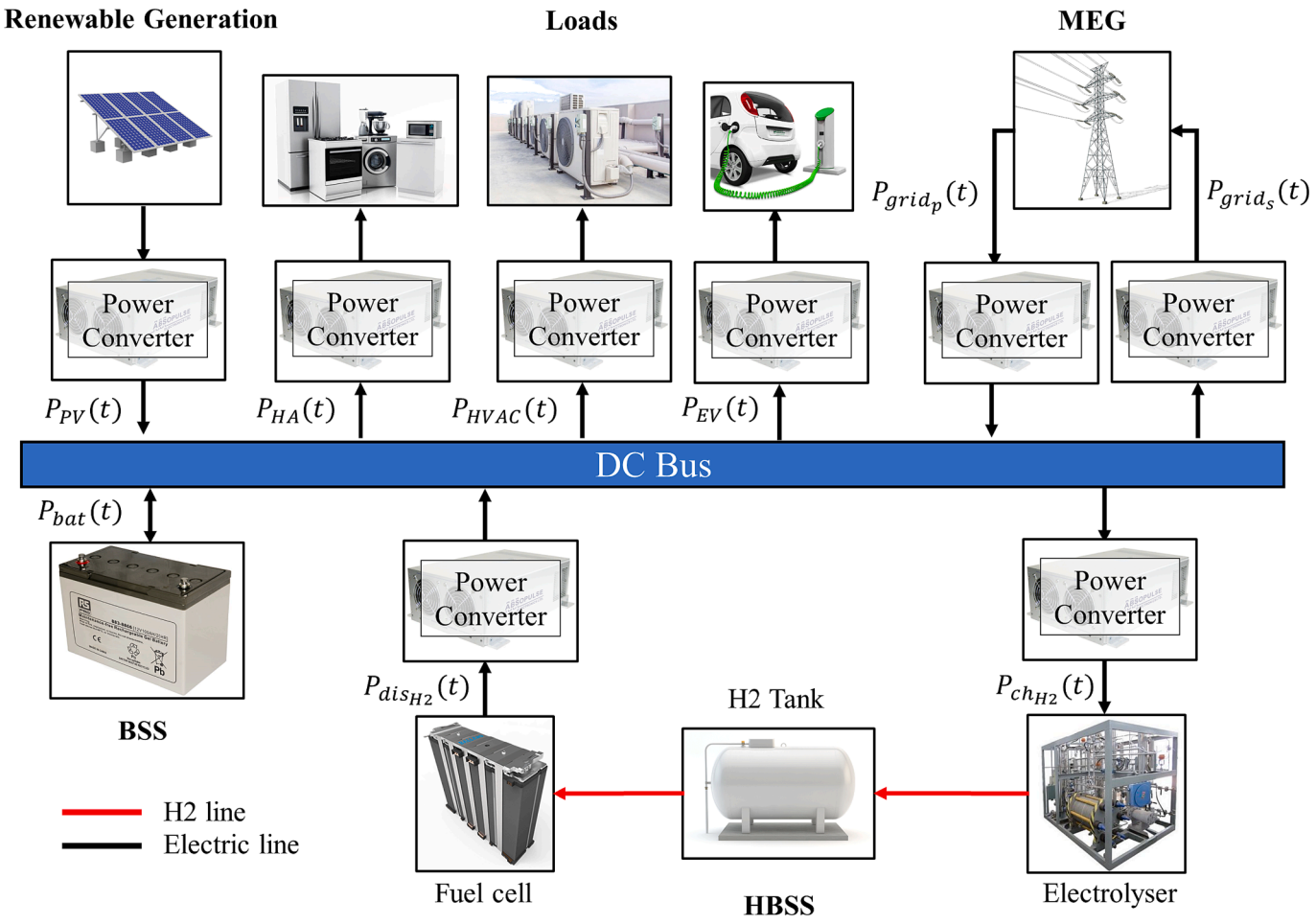

Fig. 1. Proposed microgrid architecture, illustrating the connection of renewable generation, HESS, and residential loads to the DC bus.

bus via its respective power converter.

Additionally, the microgrid features a bidirectional interface with the MEG, implemented through power converters. This connection serves to maintain power balance during periods of significant energy surplus or deficit and enables economic optimisation through energy trading with the MEG, allowing both import and export of electricity.

2.2. Modelling

Following the definition of energy flows within the microgrid architecture (Fig. 1), it is essential to develop a system model that supports the implementation of effective control strategies. Since the primary aim of this study is to demonstrate the technical feasibility of the proposed algorithm and to compare its performance against conventional control approaches, model uncertainties are intentionally excluded from the analysis. Accordingly, a deterministic representation of the plant is adopted.

This section presents the main components of the deterministic microgrid model, with detailed modelling procedures adapted from prior work [11]. The model is designed to balance accuracy with computational efficiency by employing a piecewise linear approximation. This technique captures the system's inherent nonlinearities while accounting for key aspects such as power flow direction, the configuration of the DC bus, and the presence of multiple energy storage systems (ESSs).

In this modelling approach, as illustrated in Fig. 1, the net power flow for each ESS, including both the BSS (bat) and HBSS (H_2) is defined as $P_j = P_{dis_j} - P_{ch_j}$, where $j \in \{bat, H_2\}$. Here, P_{ch_j} and P_{dis_j} represent the charging and discharging powers of ESS j, respectively. Similarly, the power exchange with the MEG is defined as $P_{grid} = P_{grid_p} - P_{grid_s}$, where P_{grid_p} and P_{grid_s} denote the power purchased from and sold to the MEG, respectively.

This formulation serves as the foundation for the comprehensive microgrid model that captures the dynamic of the ESS, the control of the DC bus voltage (V_{BUS}) when necessary, and the power balance that governs the microgrid operation, regardless of whether the system is islanded or grid-connected.

Irrespective of the ESS type or the direction of power flow, the system dynamics can be accurately described by an energy balance using a first-order discrete-time integrator, as supported by prior studies [5,11]. Consequently, the dynamic behaviour of both the BSS and HBSS is represented by Eq. (1).

$$SOC_j(k+1) = SOC_j(k) + r_{ch_j} \cdot P_{ch_j}(k) - r_{dis_j} \cdot P_{dis_j}(k) \quad (1)$$

The charging and discharging ratios for each ESS, denoted as r_{chj} and r_{dis_j}, are derived from the energy balance equation. These ratios depend on the nominal capacity CN_j (in Wh), charging and discharging efficiencies η_{ch_j} and η_{dis_j}, and the sampling time (T_S), as shown in Eq. (2).

$$r_{chj} = \frac{\eta_{ch_j}}{CN_j} \cdot T_s ; r_{dis_j} = \frac{1}{\eta_{dis_j} \cdot CN_j} \cdot T_s \quad (2)$$

The inclusion of the DC bus voltage variable (V_{BUS}) is particularly important in microgrid architectures where an ESS, typically a BSS, is directly responsible for voltage support and regulation [11,52]. In such context, V_{BUS} is introduced as an additional state variable. Based on the proposed microgrid architecture (Fig. 1), a linearised dynamic model of

V_{BUS} is derived as a function of the BSS power, following the general form described in Eq. (3) [11].

$$V_{BUS}(k+1) \approx K_{V_{BUS}} \bullet V_{BUS}(k) + K_{SOC} \cdot SOC_{bat}(k) + K_{Pch} \cdot P_{ch_{bat}}(k) - K_{Pdis} \cdot P_{dis_{bat}}(k) + v_k \tag{3}$$

In this expression, the parameters $K_{V_{BUS}}$, K_{SOC}, K_{Pch} and K_{Pdis} represent the coefficients associated with the battery's contribution to V_{BUS}, the state of charge SOC_{bat}, charging power $P_{ch_{bat}}$, and discharging power $P_{dis_{bat}}$, respectively. The constant term v_k accounts for the offset introduced during linearisation process.

Given that the dynamic behaviour of the microgrid is primarily governed by the ESS, equations (1)-(3) can be collectively represented in a standard state-space form as $x(k+1) = Ax(k) + bu(k) + d$, as shown in Eq. (4). The model is intentionally designed to be modular and scalable, allowing for the integration of additional components by extending the state vector and associated dynamics accordingly.

$$\overbrace{\begin{bmatrix} SOC_{bat}(k+1) \\ SOC_{H2}(k+1) \\ V_{BUS}(k+1) \end{bmatrix}}^{x(k+1)} = \overbrace{\begin{bmatrix} 1 & 0 & 0 \\ 0 & 1 & 0 \\ K_{SOC} & 0 & K_{V_{BUS}} \end{bmatrix}}^{A} \overbrace{\begin{bmatrix} SOC_{bat}(k) \\ SOC_{H2}(k) \\ V_{BUS}(k) \end{bmatrix}}^{x(k)} + \overbrace{\begin{bmatrix} r_{ch_{bat}} & -r_{dis_{bat}} & 0 & 0 \\ 0 & 0 & r_{ch_{H2}} & -r_{dis_{H2}} \\ K_{Pch} & -K_{Pdis} & 0 & 0 \end{bmatrix}}^{B} \overbrace{\begin{bmatrix} P_{ch_{bat}}(k) \\ P_{dis_{bat}}(k) \\ P_{ch_{H2}}(k) \\ P_{dis_{H2}}(k) \end{bmatrix}}^{u(k)} + \overbrace{\begin{bmatrix} 0 \\ 0 \\ v_k \end{bmatrix}}^{d} \tag{4}$$

3. Move-Blocking MPC-based EMS control of microgrid

As previously mentioned, EMS for a microgrid must address both short-term operational aspects, such as system dynamics, HESS constraints, and fluctuations in generation and demand, and long-term objectives, particularly operating cost optimisation. However, incorporating both short- and long-term considerations within a conventional MPC framework leads to high computational complexity, which is often impractical. Additionally, microgrids operate under significant uncertainty, particularly regarding forecasts of renewable energy production and energy demand. The reliability of such forecasts is higher for time steps nearer to the present and diminishes further into the prediction horizon. Furthermore, information on energy prices is typically available only a limited time in advance and may not be known beyond certain points in time.

To address these challenges, this section introduces a novel approach based on the Move-Blocking (MB) strategy [34,53]. This methodology allows greater flexibility during the most reliable initial time steps and progressively reduces the degrees of freedom in the less certain future intervals. It facilitates the simultaneous consideration of short- and long-term aspects within a single MPC framework. Additionally, the prediction horizon can be dynamically shortened if certain data, such as energy prices, are unavailable or intentionally excluded. This strategy significantly reduces the computational burden, enhancing the feasibility of practical implementation.

Within this framework, the present study aims to demonstrate the technical feasibility of the proposed algorithm and assess its performance against conventional two-level control strategies. To isolate and highlight the fundamental capabilities of the proposed method, uncertainties related to generation and demand forecasts, as well as controller design parameters (e.g., cost coefficients), are not considered in this analysis. Nonetheless, the authors emphasise that, despite the absence of explicit uncertainty modelling, the unified formulation inherently offers greater adaptability than traditional hierarchical approaches. By performing optimisation at each sampling interval, using the most recent system information, the controller exhibits improved responsiveness to real-time events such as abrupt load changes or rapid shifts in electricity prices. In contrast, two-level architectures typically rely on a slower high-level optimisation cycle (e.g., hourly), which restricts their ability to respond promptly to such dynamic changes.

The proposed approach is illustrated in Fig. 2. At each iteration, an MPC is defined using a prediction horizon composed of multiple inner horizons H_i, each with its own sampling time T_{S_i}, such that the total prediction horizon is $PH = H_1 + H_2 + H_3 + \cdots + H_m$. In this general case (with m inner horizons), the first horizon H_1 is defined with a sampling time T_{S_1}; the next horizon H_2 with T_{S_2}; then H_3 with T_{S_3}, and so on, until the final inner horizon H_m with T_{S_m}. Typically, the sampling time increases progressively along the prediction horizon ($T_{S_1} \leq T_{S_2} \leq T_{S_3} \leq \cdots \leq T_{S_m}$).

This structure reduces computational effort by avoiding the use of fine discretisation across the entire prediction horizon. Instead, finer sampling times are reserved for the initial, more critical intervals, while coarser sampling is applied to later stages, which are subject to higher uncertainty. This allows for accurate modelling of short-term dynamics while still capturing long-term behaviour efficiently. At each iteration, only the first control action is implemented.

The PH can also vary at each iteration. For instance, it may be shortened when certain forecast data is unavailable. In particular, as the MEG operates within the daily energy pool market, price data for the following day becomes available only after a specific market closure time. Consequently, the PH must be dynamically adjusted to ensure that predictions and cost evaluations are based on accurate, available data. If a fixed 24-hour PH were used, energy prices beyond midnight of the current day would remain unknown, requiring estimations that could compromise economic performance. To avoid this, the PH is trimmed by reducing one or more of the later inner horizons (e.g., H_2, as shown in Fig. 2), while preserving higher resolution in the earlier, more reliable intervals. Once the next day's prices become available (typically after market closure), the PH can be restored.

Nonetheless, the structure of the PH, including the definition of its inner horizons and corresponding sampling intervals, should be aligned with the temporal resolution of the pricing data, which is usually hourly. If energy prices are defined in hourly bands, it is critical to ensure that no hour change occurs within a single sampling period. For example, suppose H_3 starts at 21:30 h with a sampling period $T_{S_3} = 1h$. In this case, it spans 21:30–22:30 h, overlapping two price bands: 21:00–22:00 h and 22:00–23:00 h. Since the applicable price for the full interval is unknown, it becomes unclear how to allocate the cost of energy bought or sold. Therefore, sampling periods must be designed such that they align with hourly pricing intervals.

Once the control approach is defined, the cost function to be minimised by the MPC is introduced. Several types of cost functions have been proposed in prior research [24,54], including economic and weighted-sum indices. For consistency in comparing the two approaches evaluated in this study (the MB method and the hierarchical approach), the general economic index outlined in [11] is adopted, as defined in Eq. (5). This index expresses all variables in economic terms and is designed to be parameterisable, intuitive, and easy to interpret. Its flexibility and generality render it applicable across a wide range of microgrid

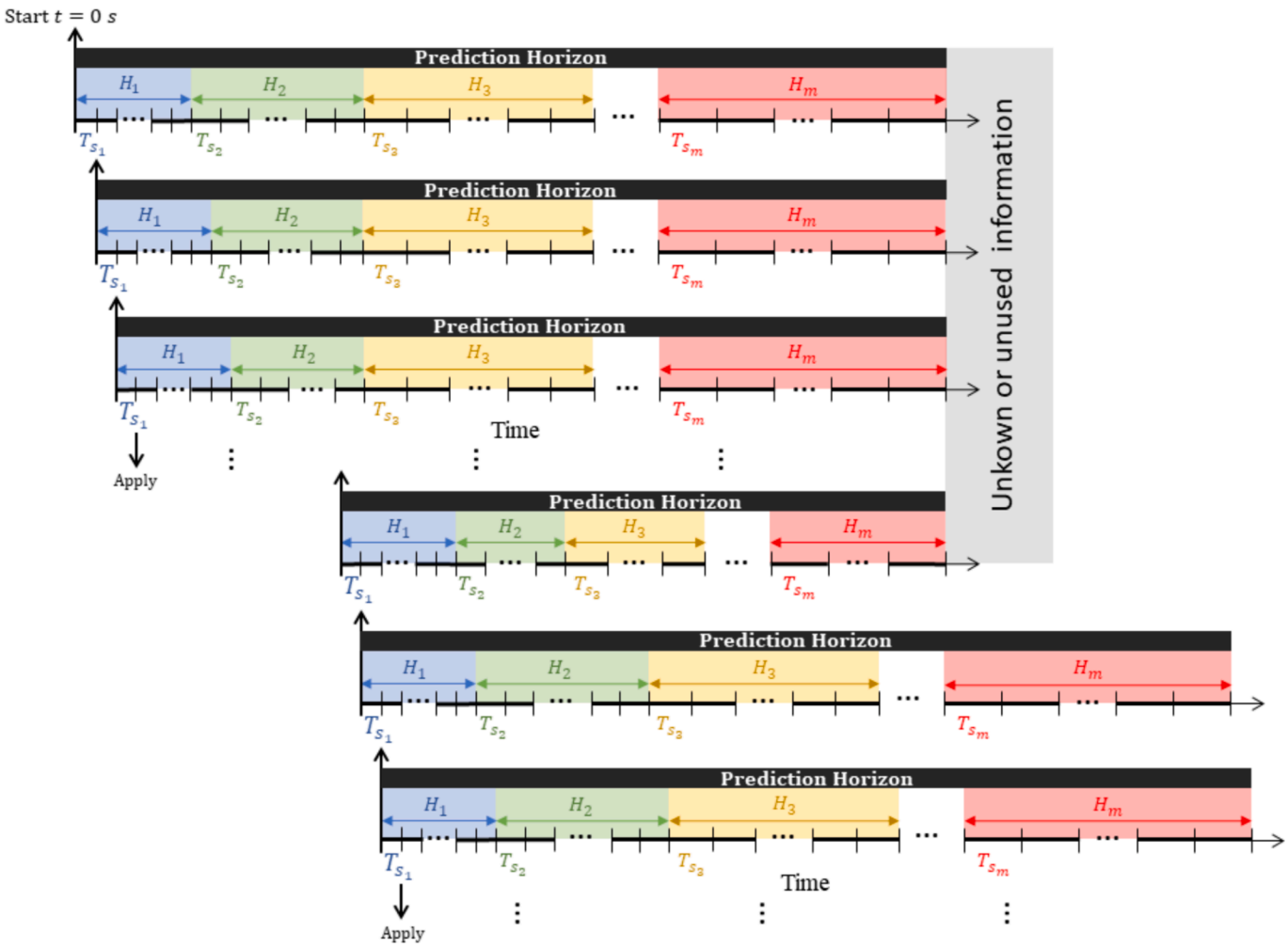

Fig. 2. Schematic of the proposed motion blocking strategy with the inner horizons and their sampling times.

configurations, as it can be adapted to reflect the specific characteristics of integrated devices, including their efficiency and operating costs. Specifically, the index defined in Eq. (5) accounts for time-dependent data at each time step k within the PH, as well as the operating costs of both ESS and MEG components.

$$J = \sum_{k=1}^{PH} \sum_{i=MEF}^{|MEF|} C_i^{var}(k) \cdot P_i(k) \cdot T_s(k) + C_i^{fix}(k) \cdot WT_i(k) \cdot T_s(k) + C_i^{start} \cdot Start_i(k) + C_i^{degr} \cdot \delta P_i^2(k) \quad (5)$$

Where $C_i^{var}, C_i^{fix}, C_i^{start}$ and C_i^{degr} represent the variable, fixed, start-up, and degradation costs of MEF_i respectively. The binary variable $WT_i(k)$ indicates whether device i is operating at time step k, and $Start_i(k)$ is a binary variable that denotes whether device i is being switched on at time k. The variable δP_i represents the power variation across all time steps, except during transitions from the start-up to the energised states or from energised to shutdown states of MEF_i.

It is important to note that, depending on the inner horizon H_i active at each instant k, both the powers P_i and the binary decision variable WT_i may be applied over differing durations, as determined by the sampling time T_{S_i}. Consequently, the variable and fixed cost terms C_i^{var} and C_i^{fix} are dependent on T_{S_i}, and thus vary with each time instant k. A distinct cost is therefore defined for each inner horizon composing the PH.

In contrast, the start-up cost C_i^{start}, degradation cost C_i^{degr}, and their associated decision variables $Start_i$ and δP_i are independent of the duration over which they are applied.

According to (5), the term $C_i^{var}(k) \cdot P_i(k)$ defines the variable operating costs of each MEF_i when operating at power level (P_i). The term $C_i^{fix}(k) \cdot WT_i(k)$ captures the fixed operational costs incurred whenever MEF_i is active, as indicated by the binary variable WT_i.

Similarly, the term $C_i^{start}(k) \cdot Start_i(k)$ accounts for the start-up costs of each MEF_i, where the binary variable $Start_i$ equals 1 if the device is activated at time k. This can be defined as $Start_i(k) = WT_i(k) \bigwedge WT_i(k-1)$, indicating a transition from an off state to an on state.

In microgrids applications, frequent switching on and off of components such as fuel cells or electrolysers can substantially shorten their operational lifespan. To mitigate this, additional penalties may be introduced to discourage excessive switching activity.

Finally, the term $C_i^{degr}(k) \cdot \delta P_i^2(k)$ represents the degradation cost associated with fluctuations in the power output of MEF_i. Since frequent variations in output power are undesirable, particularly when balancing variable generation and demand, this cost term penalizes such behaviour. However, fluctuations occurring during start-up or shutdown periods should not be penalised [11,55]. To this end, the power variation δP_i is conditioned by the binary variable Y_i, which indicates whether MEF_i is undergoing start-up or shutdown process. Specifically, $Y_i = 0$ during start-up or shutdown periods, as determined by the sampling intervals required to reach nominal operating conditions or complete shutdown. This duration is defined by the parameter NT_{Si}, as formalised in Eq. (6):

$$\delta P_i = \Delta P_i \cdot Y_i$$

Where:

$$Y_i = (WT_i(k) \wedge WT_i(k-1) \wedge \cdots \wedge WT_i(k-NT_{Si})) \quad (6)$$

4. Bilevel hierarchical MPC-based EMS

As previously stated, the primary objective of the present study is to develop a computationally efficient MB-MPC-based EMS, aimed at improving economic performance relative to computationally tractable solutions commonly found in the literature. To validate this approach, a comparative performance analysis is conducted between the proposed MB-MPC framework and a widely adopted bilevel hierarchical MPC-based EMS, hereafter referred to as the bilevel approach. The latter is specifically designed to minimise the operating costs of the microgrid.

The Bilevel MPC framework comprises two interconnected control layers: a high-level (HL) controller and a low-level (LL) controller. This hierarchical structure is the most frequently implemented in recent literature [25,27], wherein the HL controller performs long-term economic optimisation, while the LL controller strictly tracks the reference provided by the HL layer.

Consistent with bilevel control principles, the HL controller operates with a relatively long sampling period Ts_{HL} and prediction horizon PH_{HL}. At this level, average forecasts of renewable energy generation and load demand are used to determine the mean energy exchange required from each component of the microgrid withing each sampling interval. This ensures power balance according to the formulation in Eq. (5). However, due to the coarse temporal resolution, the HL controller lacks detailed information on intra-period dynamics. This temporal abstraction may limit the economic optimality of the resulting energy dispatch decisions.

To address this limitation, the LL controller operates with a shorter sampling period T_{SLL} and a shorter prediction horizon PH_{LL}, enabling it to perform short-term refinements of the HL's set-points. At each sampling instance, the LL controller solves a constrained optimal tracking problem using the reference trajectories for state and control variables provided by the HL. This ensures that the system dynamics are accurately tracked in the short term, thereby enhancing control and system responsiveness.

4.1. High level

The HL controller is responsible for formulating the most economically advantageous operational strategy based on long-term forecast of renewable generation and demand. with determining the most economically efficient strategy for the microgrid. This is accomplished using a reduced-order state-space model of the microgrid, wherein the state variable V_{BUS}, associated with voltage dynamics, is omitted, as voltage control is not relevant for long-term energy scheduling. The HL thus solves an economic optimisation problem, yielding optimal reference trajectories for power flows, SOC values, and operational cycles to be followed by the LL controller. This optimisation is performed over the prediction horizon PH_{HL} using averaged data inputs. In this manuscript, this controller will be referred to as "HL controller".

Regarding the cost function, previous works have adopted various economic and weighted objective functions. To ensure a fair and consistent comparison between the MB-MPC and bilevel approaches, this study adopts the generic economic cost index introduced in [11], defined in Eq. (7). This index is evaluated over the HL sampling period (T_{SHL}) and prediction horizon (PH_{HL}), and explicitly incorporates the operational characteristics of both the HBSS and the MEG at each time step k. The subsequent sections provide a detailed description of the HL and LL controllers.

4.2. Low level

The LL tracking strategy is designed to minimise the operational cost of the microgrid while managing power flows and mitigating discrepancies between the forecasted and actual generation and demand profiles that may arise between T_{SHL}. Additionally, the LL is responsible for the short-term regulation of the DC bus voltage. To accomplish this, the LL utilizes the complete state-space model of the microgrid, as described in Eq. (4), to execute a tracking strategy that accurately follows the references provided by the HL within a shorter sampling period. Typically, the prediction horizon of the LL (PH_{LL}) is chosen to match with HL sampling period ($PH_{LL} = T_{SHL}$). In this manuscript, this controller will be referred to as "LL controller".

In line with common practice in the literature, this study adopts the generic tracking-oriented cost index for the LL controller, as defined in Eq. (7) [17,56]. In this formulation, index i corresponds to the HESS and the MEG, specifically the battery charging/discharging ($P_{ch_{bat}}$, $P_{dis_{bat}}$), hydrogen charging/discharging ($P_{ch_{H2}}$, $P_{dis_{H2}}$), and grid import/export (P_{grid_p}, P_{grid_s}), while index j refers to the storage devices, either the BSS (bat) or HBSS (H2). Certain terms may be omitted in practice by assigning zero-weighting factors, thereby maintaining the flexibility of the formulation.

$$J = \sum_{k=1}^{PH_{LL}} \left(\left(\sum_i \omega_{P_i} \left(P_i(k) - P_i^{ref} \right)^2 + \omega_{Start_i} \cdot Start_i(k) + \omega_{\delta P_i} \cdot \delta P_i{}^2(k) \right) + \sum_j \left(\omega_{SOC_j} \left(SOC_j(k) - SOC_j^{ref} \right)^2 \right) \right) \quad (7)$$

This cost index evaluates the relevant variables at each time step k within the PH_{LL}, including the power flows associated with the HESS and the MEG. It is designed to enhance performance through a set of weighted objectives, which reflect the microgrid's operational priorities. These terms include weights for power variables (ω_{P_i}), startup events (ω_{Start_i}), power fluctuations ($\omega_{\delta P_i}$), and SOC (ω_{SOC_j}).

As specified in Eq. (7), the first term of the index ensures accurate tracking of the HL power references for both the HESS and MEG. Beyond reference tracking, conservative operation of the HESS is vital, as excessive cycling, particularly of the HBSS, can adversely impact its lifespan. Therefore, similar to the economic cost function used by the HL controller, the second term of the LL cost index discourages frequent start-stop transitions in HBSS components. The third term promotes smooth operation by penalising large fluctuations, and the final term incentivises SOC values that remain close to the HL-provided references, thereby supporting coherent coordination between the HL and LL control layers.

5. Optimisation problem

Irrespective of the specific EMS strategy of cost index employed, the formulation of the control problem requires the definition of constraints. These include an equality constraint related to power balance, inequality constraints governing the state and control variables, and the mathematical formulation to the underlying optimisation problem. These components will be discussed in detail in the subsequent sections.

5.1. Constraints

The constraints of the optimisation problem are categorised into two main types. The first is the fundamental power balance equality constraint, which governs the entire system. The second is a set of inequality constraints that represent the specific operational limits of each component.

5.1.1. Power balance

In accordance with standard practices in electrical power systems, the microgrid must ensure energy balance, as described by the power balance constraint in Eq. (8) [11,57]. This equation accounts for energy conversion losses and auxiliary consumption, collectively referred to as "losses"). It imposes an equality constraint that enforces the power

balance at the DC internal bus of the microgrid. This balance must be maintained exclusively through controllable power flows, namely those associated with the HESS and the MEG.

Consistent with the modelling assumptions introduced in Section 2, all power variables are treated as strictly positive quantities at the component level. However, in the context of the power balance equation, the signs of these variables must reflect whether power is being injected into or drawn from the DC bus. Consequently, the powers injected into the DC bus (P_{grid_p}, P_{dis_j} and P_{PV}) are accounted as positive, whereas the powers extracted from the bus (P_{grid_s}, P_{ch_j} and P_{Load}) are designated as negative.

$$P_{PV}(k) - P_{Load}(k) - Loss(k) + P_{grid}(k) + P_{bat}(k) + P_{H_2}(k) = 0 \tag{8}$$

Where sign of the power associated with ESS (P_{bat} and P_{H2}) and MEG (P_{grid}) is determined by the previously defined expressions: $P_{grid} = P_{grid_p} - P_{grid_s}$ and $P_j = P_{dis_j} - P_{ch_j}$, where the index $j \in \{bat, H_2\}$ refers to the BSS (bat) and HBSS (H_2), respectively.

The term $Loss(k)$ denotes the total internal losses of the microgrid at time step k, specifically those not already embedded in the renewable generation or load terms. Since the net energy flows to and from the DC bus already account for the corresponding losses in generation and demand, $Loss(k)$ is defined to include only the losses associated with the operation of the HESS and MEG (Fig. 1), as formalised in Eq. (9).

$$Loss(k) = \sum Loss_i(k) \cdot P_i(k) + Loss_i^{BoP} \cdot WT_i \tag{9}$$

According to Eq. (9), $Loss(k)$ are composed of two components: Variable conversion losses, denoted as $Loss_i$, expressed as a percentage of the operating power P_i of the device, representing losses due to power electronics and conversion inefficiencies; Fixed auxiliary (balance-of-plant) losses, represented as $Loss_i^{BoP}$, which represent static consumption incurred by balance-of-plant components during operation.

The index $i \in \{ch_{bat}, dis_{bat}, ch_{H2}, dis_{H2}, grid_p, grid_s\}$ denotes the specific operational mode of the BSS, HBSS, or MEG. Furthermore, the binary variable $WT_i \in \{0,1\}$ indicates the operational status of each unit, where $WT_i = 1$ if the unit is active and $WT_i = 0$ otherwise.

5.1.2. Operating constraints

As previously stated, the principal objective of the EMS is to maintain power balance on the DC bus, as defined by Eq. (8). Achieving this objective requires the careful integration of various physical and operational constraints that influence the performance of each system component. Once the control-oriented model and cost function have been formulated for each EMS strategy, it becomes essential to define the set of constraints that will govern the microgrid's operation. These constraints pertain to the control variables and are derived from device-specific operational limits and manufacturer-recommended guidelines, thereby ensuring the safe and efficient functioning of the systems. Additionally, certain constraints reflect conservative operating modes adopted for specific subsystems, such as the HBSS, to enhance operational robustness and reliability.

The first set of constraints typically addresses the physical limitations inherent in each device, including established minimum and maximum power thresholds ($\underline{P_i}$ and $\overline{P_i}$, respectively) that must not be exceeded ($\underline{P_i} \le P_i \le \overline{P_i}$). Furthermore, constraints on the minimum and maximum permissible variation in power ($\underline{\Delta P_i}$ and $\overline{\Delta P_i}$, respectively) are introduced to impose restrictions on dynamic device behaviour

Table 1
Definition of the model, cost function, decision variables, and constraints for MB-MPC, HL and LL controllers.

Controller	Model
HL controller	$\begin{bmatrix} SOC_{bat}(k+1) \\ SOC_{H2}(k+1) \end{bmatrix} = \begin{bmatrix} 1 & 0 \\ 0 & 1 \end{bmatrix} \begin{bmatrix} SOC_{bat}(k) \\ SOC_{H2}(k) \end{bmatrix} + \begin{bmatrix} r_{ch}^{bat} & -r_{dis}^{bat} & 0 & 0 \\ 0 & 0 & r_{ch}^{H2} & -r_{dis}^{H2} \end{bmatrix} \begin{bmatrix} P_{ch_{bat}}(k) \\ P_{dis_{bat}}(k) \\ P_{ch_{H2}}(k) \\ P_{dis_{H2}}(k) \end{bmatrix}$
MB-MPC & LL controller	$\begin{bmatrix} SOC_{bat}(k+1) \\ SOC_{H2}(k+1) \\ V_{BUS}(k+1) \end{bmatrix} = \begin{bmatrix} 1 & 0 & 0 \\ 0 & 1 & 0 \\ K_{SOC} & 0 & K_{V_{BUS}} \end{bmatrix} \begin{bmatrix} SOC_{bat}(k) \\ SOC_{H2}(k) \\ V_{BUS}(k) \end{bmatrix} + \begin{bmatrix} r_{ch}^{bat} & -r_{dis}^{bat} & 0 & 0 \\ 0 & 0 & r_{ch}^{H2} & -r_{dis}^{H2} \\ K_{Pch} & K_{Pdis} & 0 & 0 \end{bmatrix} \begin{bmatrix} P_{ch_{bat}}(k) \\ P_{dis_{bat}}(k) \\ P_{ch_{H2}}(k) \\ P_{dis_{H2}}(k) \end{bmatrix} + \begin{bmatrix} 0 \\ 0 \\ 0 \\ v_k \end{bmatrix}$
	Cost function
MB-MPC	$J = \sum_{k=1}^{PH} \sum_{i=MEF}^{\lvert MEF \rvert} C_i^{var}(k) \cdot P_i(k) \cdot T_s(k) + C_i^{fix}(k) \cdot WT_i(k) \cdot T_s(k) + C_i^{start} \cdot Start_i(k) + C_i^{degr} \cdot \delta P_i^2(k)$
HL controller	$J = \sum_{k=1}^{PH_{HL}} \sum_{i=MEF}^{\lvert MEF \rvert} C_i^{var}(k) \cdot P_i(k) \bullet Ts_{HL} + C_i^{fix}(k) \cdot WT_i(k) \bullet Ts_{HL} + C_i^{start} \cdot Start_i(k)$
LL controller	$J = \sum_{k=1}^{PH_{LL}} \left(\left(\sum_i \omega_{P_i} \left(P_i(k) - P_i^{ref} \right)^2 + \omega_{Start_i} \cdot Start_i(k) + \omega_{\delta P_i} \cdot \delta P_i{}^2(k) \right) + \sum_j \left(\omega_{SOC_j} \left(SOC_j(k) - SOC_j^{ref} \right)^2 \right) \right)$
	Decision variables
All MPCs	$P_{ch_{bat}}(k), P_{dis_{bat}}(k), P_{ch_{H2}}(k), P_{dis_{H2}}(k), P_{grid_s}(k), P_{grid_p}(k), WT_{ch_{bat}}(k), WT_{ch_{H2}}(k), WT_{dis_{H2}}(k), WT_{grid_p}(k), Start_{ch_{H2}}(k), Start_{dis_{H2}}(k), \delta P_{ch_{H2}}(k)^*(Y_{ch_{H2}}(k)), \delta P_{dis_{H2}}(k)^*(Y_{dis_{H2}}(k)),$ $SOC_{bat}(k), SOC_{H2}(k), V_{BUS}(k)^*$
	Constraints
All MPCs	$\underline{P_{ch_{bat}}} \cdot WT_{ch_{bat}}(k) \le P_{ch_{bat}}(k) \le \overline{P_{ch_{bat}}} \cdot WT_{ch_{bat}}(k) \underline{P_{dis_{bat}}} \cdot (1 - WT_{ch_{bat}}(k)) \le P_{dis_{bat}}(k) \le \overline{P_{dis_{bat}}} \cdot (1 - WT_{ch_{bat}}(k)) \underline{P_{ch_{H2}}} \cdot WT_{ch_{H2}}(k) \le P_{ch_{H2}}(k)$ $\le \overline{P_{ch_{H2}}} \cdot WT_{ch_{H2}}(k) \underline{P_{dis_{H2}}} \cdot WT_{dis_{H2}}(k) \le P_{dis_{H2}}(k) \le \overline{P_{dis_{H2}}} \cdot WT_{dis_{H2}}(k) \underline{P_{grid_p}} \cdot WT_{grid_p}(k) \le P_{grid_p}(k) \le \overline{P_{grid_p}} \cdot WT_{grid_p}(k) \underline{P_{grid_s}} \cdot \left(1 - WT_{grid_p}(k)\right) \le P_{grid_s}(k) \le \overline{P_{grid_s}} \cdot \left(1 - WT_{grid_p}(k)\right)$
	$SOC_j(k+1) = SOC_j(k) + r_{ch_j} \cdot P_{ch_j}(k) - r_{dis_j} \cdot P_{dis_j}(k);$
	$\underline{SOC_j} \le SOC_j(k) \le \overline{SOC_j}$
	$V_{BUS}(k+1)^* = K_{V_{BUS}} \cdot V_{BUS}(k) + K_{SOC} \cdot SOC_{bat}(k) + K_{P_{ch}} \cdot P_{ch_{bat}}(k) - K_{P_{dis}};$
	$\underline{V_{BUS}} \le V_{BUS}(k) \le \overline{V_{BUS}}^*$
	$\underline{\Delta P_{els}} \le \Delta P_{els}(k) \le \overline{\Delta P_{els}}; \underline{\Delta P_{fc}} \le \Delta P_{fc}(k) \le \overline{\Delta P_{fc}};$
	$Start_i(k) = WT_i(k) \wedge WT_i(k-1); \delta P_i(k) = \Delta P_i(k) \wedge Y_i(k)^*$, *with*
	$Y_i(k) = WT_i(k) \wedge WT_i(k-1)$
	$P_{dis_{bat}}(k)(1 + Loss_{dis_{bat}}) - P_{ch_{bat}}(k)(1 + Loss_{ch_{bat}}) + P_{dis_{H2}}(k)(1 + Loss_{dis_{H2}}) + WT_{dis_{H2}}(k) \cdot Loss_{dis_{H2}}^{BoP} - P_{ch_{H2}}(k)(1 + Loss_{ch_{H2}})$ $+ WT_{ch_{H2}}(k) \cdot Loss_{ch_{H2}}^{BoP} + P_{grid_s}(k)(1 + Loss_{grid_s}) - P_{grid_p}(k)\left(1 + Loss_{grid_p}\right) + P_{PV}(k) - P_{Load} = 0$

*Not considered for HL controller.

Table 2
Main electrical and operational parameters of the HESS.

ESS parameters					
BSS	$CN_{bat} = 14.4\ kWh$		$\eta_{ch}^{bat} = 0.934$		$\eta_{dis}^{bat} = 1$
	$K_{V_{BUS}} = 0.01$	$K_{SOC} = 30$	$K_{Pch} = 0.002$	$K_{Pdis} = 0.002$	$v_k = 355$
HBSS	$CN_{H2} = 12\ kWh$		$\eta_{ch}^{H2} = 0.7$		$\eta_{dis}^{H2} = 0.5$

($\underline{\Delta P_i} \leq \Delta P_i \leq \overline{\Delta P_i}$). These limitations are particularly significant for the HBSS, where excessive power fluctuations can lead to accelerated wear and degradation.

Moreover, it is essential to impose constraints that govern the operational processes conducted at any sample time k. This consideration is particularly significant for devices where it is either physically impossible or inadvisable to engage in simultaneous charging and discharging operations, or to conduct concurrent energy transactions with

Table 3
Summary of key parameters, economic cost, constraints, and losses used in the MPC formulation.

MPC Parameters & Constraints								
MEF_i	$C_i^{var}(€/MWh)$	$C_i^{fix}(€/h)$	$C_i^{start}(€)$	$C_i^{degr}(€/W^2)$	$\left[\underline{P_i}, \overline{P_i}\right](kW)$	$\left[\underline{\Delta P_i}, \overline{\Delta P_i}\right](kW)$	$Loss_i(-)$	$Loss_i^{BoP}(W)$
ch_{bat}	0.4	–	–	–	[0, 6]	[-6, 6]	–	–
dis_{bat}	0.4	–	–	–	[0, 8]	[-8, 8]	–	–
ch_{H2}	–	0.015	0.05	3.1e-9*	[1,5]	[-5, 5]	0.05	800
dis_{H2}	–	0.028	0.05	8e-9*	[1, 3.5]	[-3.5, 3.5]	0.05	300
$grid_p$	Table 4	–	–	–	[0, 8]	[-8, 8]	0.05	–
$grid_s$	Table 4	–	–	–	[0, 6]	[-6, 6]	0.05	–
State Vector Constraints								
$\overline{SOC_{bat}} = 90\ \%$, $\underline{SOC_{bat}} = 30\%$, $\overline{SOC_{H2}} = 100\ \%$, $\underline{SOC_{H2}} = 10\ \%$, $\overline{V_{BUS}} = 450\ V$, $\underline{V_{BUS}} = 330\ V$								
Initial conditions								
$V_{BUS}(0) = 367.75V$, $SOC_{bat}(0) = 30\ \%$, $SOC_{H2}(0) = 10\ \%$								

*For the HL controller this cost is not considered ($C_{ch/dis_{H2}}^{degr} = 0$).

Table 4
Hourly electricity prices (€/kWh) from the Spanish MEG used for economic optimisation.

MEG hourly power purchase and sale price on 03/28/2024*							
Time	Price purchase/sale (€/MWh)	Time	Price purchase/sale (€/MWh)	Time	Price purchase/sale (€/MWh)	Time	Price purchase/sale (€/MWh)
00–01 h	54.84 / −0.94	06–07 h	56.13 / −1.36	12–13 h	123.11 / −1.41	18–19 h	123.23 / −0.68
01–02 h	55.83 / −1.41	07–08 h	52.77 / −0.98	13–14 h	122.35 / −1.41	19–20 h	122.63 / 1.79
02–03 h	59.01 / −1.41	08–09 h	74.99 / −1.2	14–15 h	72.77 / −1.41	20–21 h	123.42 / 1.79
03–04 h	58.11 / −1.41	09–10 h	74.20 / −1.38	15–16 h	73.14 / −1.41	21–22 h	124.61 / 1.79
04–05 h	58.35 / −1.41	10–11 h	124.26 / −1.41	16–17 h	73.98 / −1.41	22–23 h	76.35 / 1.79
05–06 h	57.87 / −1.41	11–12 h	123.88 / −1.41	17–18 h	73.63 / −1.35	23–00 h	73.38 / 0.07
*MEG hourly power purchase and sale price on 03/29/2024**							
00–01 h	58.27 / 0.37	06–07 h	60.11 / 0.34	12–13 h	126.77 / −0.94	18–19 h	131.45 / 1.54
01–02 h	58.15 / −0.9	07–08 h	60.29 / 1.38	13–14 h	126.20 / −1.01	19–20 h	131.40 / 5.28
02–03 h	59.20 / −1.02	08–09 h	83.72 / −0.12	14–15 h	75.52 / −1.04	20–21 h	142.58 / 16.06
03–04 h	59.98 / −1.05	09–10 h	83.20 / −0.57	15–16 h	76.18 / −1.12	21–22 h	149.01 / 20.01
04–05 h	60.41 / −0.98	10–11 h	128.98 / −0.61	16–17 h	79.44 / −1.12	22–23 h	91.26 / 14.17
05–06 h	60.35 / −0.69	11–12 h	126.40 / −0.73	17–18 h	78.17 / −1.00	23–00 h	91.98 / 13.21

* Available on: https://www.esios.ree.es/es/pvpc.

Table 5
Weighting factors defined for the cost index of the LL controller.

Controller setting	$\omega_{P_{ch/dis\_bat}}$	$\omega_{P_{ch/dis_{H2}}}$	$\omega_{P_{grid_{p/s}}}$	$\omega_{Start_{ch/dis_{H2}}}$	$\omega_{\delta P_{els/fc}}$	$\omega_{SOC_{bat}}$	$\omega_{SOC_{H2}}$
BA-MPC1	$\frac{1}{\overline{P_{ch/dis_{bat}}}^2}$	$\frac{1}{\overline{P_{ch/dis_{H2}}}^2}$	$\frac{1}{\overline{P_{grid_{p/s}}}^2}$	0	0	0	0
BA-MPC2	$\frac{1}{\overline{P_{ch/dis_{bat}}}^2}$	$\frac{10^2}{\overline{P_{ch/dis_{H2}}}^2}$	$\frac{10^4}{\overline{P_{grid_{p/s}}}^2}$	10^2	$\frac{10^2}{\overline{\Delta P_{els/fc}}^2}$	1	1

the MEG. Accordingly, logical constraints of the form $WT_{ch_j} + WT_{dis_j} \leq 1$ (or $WT_{gridin} + WT_{gridout} \leq 1$) restrictions will be defined accordingly, where the binary variable WT_i denotes the operational status of an energy flow path MEF_i.

Finally, constraints on the minimum and maximum values of the state variables of the microgrid ($\underline{x}$ and $\overline{x}$, respectively) are introduced ($\underline{x} \leq x(k) \leq \overline{x}$). These may include both hard physical bounds and recommended operating margins that are critical to ensure the safe, reliable, and efficient operation of the HESS and other key components of the microgrid.

5.2. Optimisation problem

Considering the preceding discussion, the MB-MPC and bilevel MPC-based EMS are formulated as the optimisation problem outlined in equation (10). In this formulation, the vector of decision variables is given by $z = [P_i(k),\ WT_i(k), Start_i(k), \delta P_i(k)]$, where each element pertains to the MEF associated with the BSS, HBSS, and MEG subsystems of the microgrid.

$$\begin{gathered} minJ \\ \text{Subject to :} \\ \underline{P_i} \cdot WT_i(k) \leq P_i(k) \leq \overline{P_i} \cdot WT_i(k) \\ \underline{\Delta P_i} \leq \Delta P_i(k) \leq \overline{\Delta P_i} \\ WT_{ch_j}(k) + WT_{dis_j}(k) \leq 1 \\ WT_{grid_s}(k) + WT_{grid_p}(k) \leq 1 \\ \underline{x} \leq x(k) \leq \overline{x} \\ x(k+1) = A \cdot x(k) + B \cdot u(k) + d \\ P_{PV}(k) - P_{Load}(k) - Loss(k) + P_{grid}(k) + P_{bat}(k) + P_{H_2}(k) = 0 \end{gathered} \tag{10}$$

In this context, J denotes the general economic cost function described in Eq. (7), which serves as the objective for both the MB-MPC and the HL controller withing the bilevel framework. In contrast, the cost function applied by the low-level (LL) controller is defined in Eq. (9), reflecting its distinct role in short-term operational tracking.

Furthermore, the constraints define: 1) the minimum and maximum power bounds for each device, 2) the power ramping limits for each device, 3) a condition to prevent simultaneous charging and discharging of ESSs, 4) a condition to prevent the simultaneous purchase and sale of energy to the grid, 5) the upper and lower bounds on the model's state variables (SOC_j and V_{BUS}), 6) the state-space model representing the system's dynamics, and 7) the power balance equation that the microgrid must meet.

Based on the designed methodology outlined in Sections 2, 3 and 4, Table 1 provides a summary of the decision variables, microgrid models,

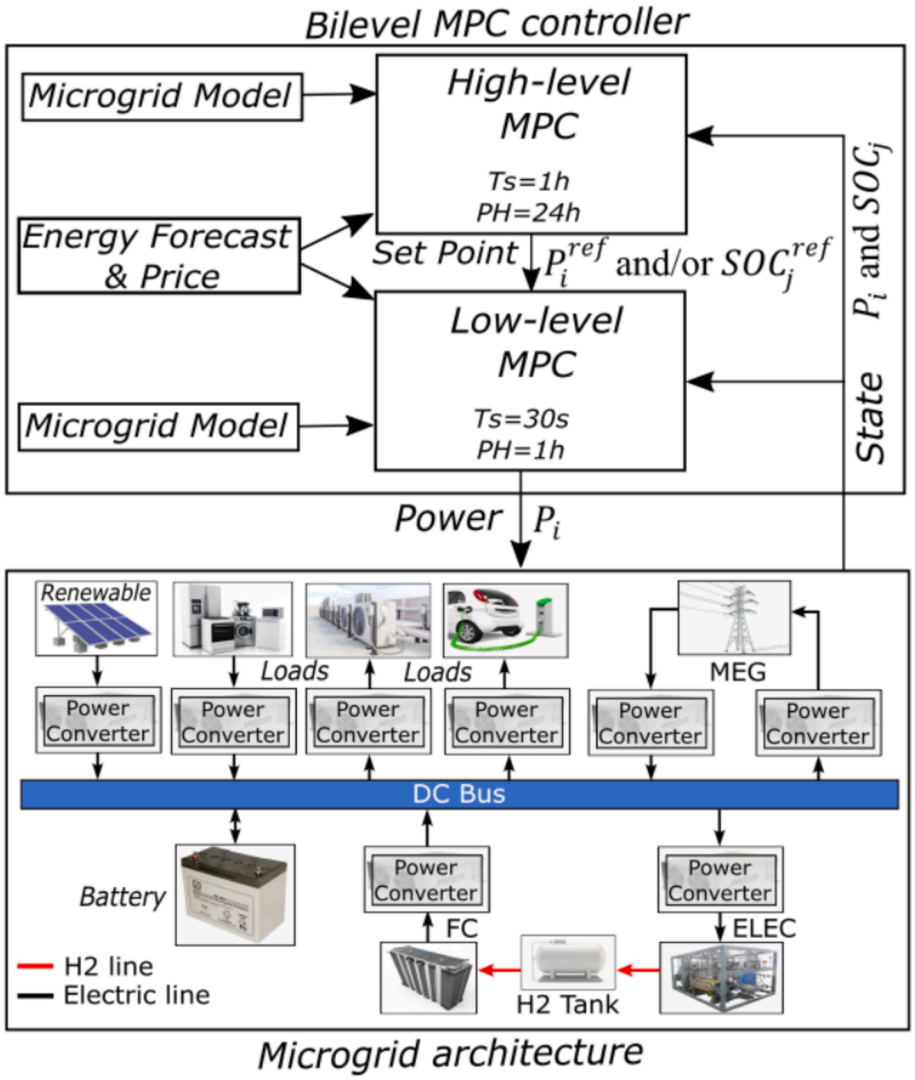

Fig. 3. Structure of the bilevel MPC controller, highlighting the interaction between the HL (economic optimiser) and the LL (power-sharing controller).

objective functions, and constraints employed in the optimisation problem for each EMS approach.

6. Case study: results & discussion

In this section, the proposed MB-MPC-based EMS is validated following the methodology outlined in Section 3. The validation process involved designing the proposed EMS approach for the microgrid architecture shown in Fig. 1 and comparing the simulation results with both the optimal case, and the most utilized approach in the literature, which is based on a hierarchical bilevel MPC, as described in Section 4.

The subsequent section introduces the case study, outlining the design parameters of the microgrid under consideration (Fig. 1), including renewable generation and demand profiles, as well as the sizing of the HESS. Additionally, it outlines the design assumptions and parameters of the evaluated EMS approaches, including sampling times, costs, weighting factors, and operational constraints.

For the formulation of the optimisation problem, a mixed-integer quadratic programming (MIQP) approach was adopted, aligned with the quadratic cost index employed across the various methods. In line with the established design methodology, the decision variables, objective functions, and constraints used in the optimisation problem are comprehensively presented in this section (Tables 3-5). Given that simulation constitutes a critical initial step in the validation of any advanced control strategy, this study focuses on assessing the performance of the proposed controller via simulation, benchmarking it against well-established reference controllers. Experimental validation is envisaged as a subsequent phase of the research, to be undertaken once access to a suitable operational pilot plant has been secured. Nonetheless, the insights gained from these simulations, grounded in realistic operating conditions, provide valuable preliminary evidence of the proposed controller's effectiveness and practical feasibility. To this end, several simulations were conducted in MATLAB Simulink®, employing the YALMIP toolbox in conjunction with the IBM CPLEX solver to resolve the MIQP formulations.

6.1. Microgrid description

The sizing of a microgrid is a multifaceted task that necessitates the consideration of numerous factors, including the availability of renewable energy resources, the load profile, and the capital and operational costs of system components. However, as the primary objective of this study is not to address microgrid sizing, the technical specifications of the components have been defined with reference to the experimental microgrid available to the authors at CITES. Further details regarding this facility are provided in [5,57].

For the purposes of this study, the renewable generation profile has been modelled using representative solar irradiance data corresponding to the summer months in Huelva, Spain. Similarly, the demand profile reflects a typical residential load pattern, based on consumption data published by the Spanish Institute for Energy Diversification and Saving (IDAE).

In accordance with the methodology and the flowchart outlined in [11], the microgrid architecture under consideration (Fig. 1) and the state-space model of the microgrid presented in Eq. (4), the key parameters of the HESS employed in this study are summarised in Table 2.

6.2. Mpc-based EMS

To formulate the MPC-based EMS approaches, it is necessary to establish the sampling periods and PH, as well as the constraints, losses, weights (in case of LL controller), and cost terms of the optimisation index associated with the HESS and MEG, in accordance with the microgrid architecture described in Section 2.

As outlined in Section 5.1 and summarised in Table 1, the constraints encompass the physical power limits or operational guidelines for the HESS (power and state variables), as well as the decision variables $Start_i$, δP_i, and Y_i, which are formulated by converting logical relations into mixed-integer inequalities [11]. In addition, the MPCs parameters, costs values (HL and MB-MPC controllers), constraints, and losses are defined in Table 3. As previously stated, the selection of these constraint values is based on the physical system limitations and manufacturer-recommended operating conditions, ensuring the safe and efficient operation of components. Specifically, for the microgrid under study, the values are derived from representative parameters observed in similar microgrid architectures reported in the scientific literature [11,55].

Regardless of the MPC approach under examination, a common set of fixed, variable, start-up, and degradation costs for the HESS and MEG are considered. These cost parameters, summarised in Table 3, are based on typical average values documented in previous studies [11,55]. The rationale for including or omitting specific cost components for each element will be explained in the subsequent sections.

For the BSS, only variable costs associated with operation and maintenance are included. Due to its direct integration with the DC bus, no energy conversion losses are considered, as power converters are not required.

In the case of the HBSS, fixed costs related to operation and maintenance, start-up costs, and degradation costs are all accounted for. However, variable costs are omitted, as the auxiliary energy consumption is already incorporated within the power balance described by Eq. (5). Regarding losses, the HBSS is subject to both variable losses resulting from energy conversion within power electronic converters, and fixed losses associated with the auxiliary consumption of the electrolyser and fuel cell balance-of-plant (BoP) systems. These values are based on actual equipment specifications.

Finally, for the MEG, bidirectional operation is associated solely with variable operating costs, which correspond to energy purchasing and selling prices. These are detailed in Tables 3 and 4, and are based on market data for the Iberian Peninsula (Spain) as of 28 and 29 March 2024. Notably, energy sale prices may be either positive, yielding a profit, or negative, indicating that exporting energy incurs a cost. Unlike the BSS, the MEG is connected to the DC bus via power converters, and thus experiences variable energy conversion losses.

6.2.1. Bilevel approach

This approach is illustrated in Fig. 3. The sampling periods and prediction horizons used in the bilevel control strategy were selected based on the dynamic characteristics of the microgrid components, the discretization intervals of electricity purchase/sale prices from the MEG, and the typical generation and consumption profiles observed in residential microgrids. These choices are consistent with common practices in the design of hierarchical MPC-based EMS frameworks reported in the scientific literature [24,26].

Following this rationale, the HL controller is configured with a prediction horizon of $PH_{HL} = 24h$ and a sampling period of $T_{SHL} = 1h$. The LL controller, in contrast, operates with a prediction horizon of $PH_{LL} = 1h$ and a sampling period of $T_{SLL} = 30\,sec$. The HL controller is optimised every T_{SHL}, while the LL controller is updated every T_{SLL}.

At the start of the scenario (00 h on March 28), only energy prices up to 00 h on March 29 are available. As a result, PH_{HL} must be truncated accordingly: at 00 h $PH_{HL} = 24h$, at 01 h $PH_{HL} = 23h$, at 02 h $PH_{HL} = 22h$, and so on. By 21 h, the energy prices for March 29 become accessible, allowing the PH_{HL} to be restored to its full duration of 24 h ($PH_{HL} = 24h$), which is maintained until the end of the scenario (00 h on March 29).

Both the HL and LL controllers minimise their respective indices as defined in Table 1 (see Eqs. (5) and (7), respectively). The cost structure for the HL controller is outlined in Table 3, while the weighting factors used by the LL controller are provided in Table 5. Unlike the MB-MPC and the HL controller, the LL controller solves a weighted multi-objective tracking problem (refer to Eq. (7)). As discussed in the

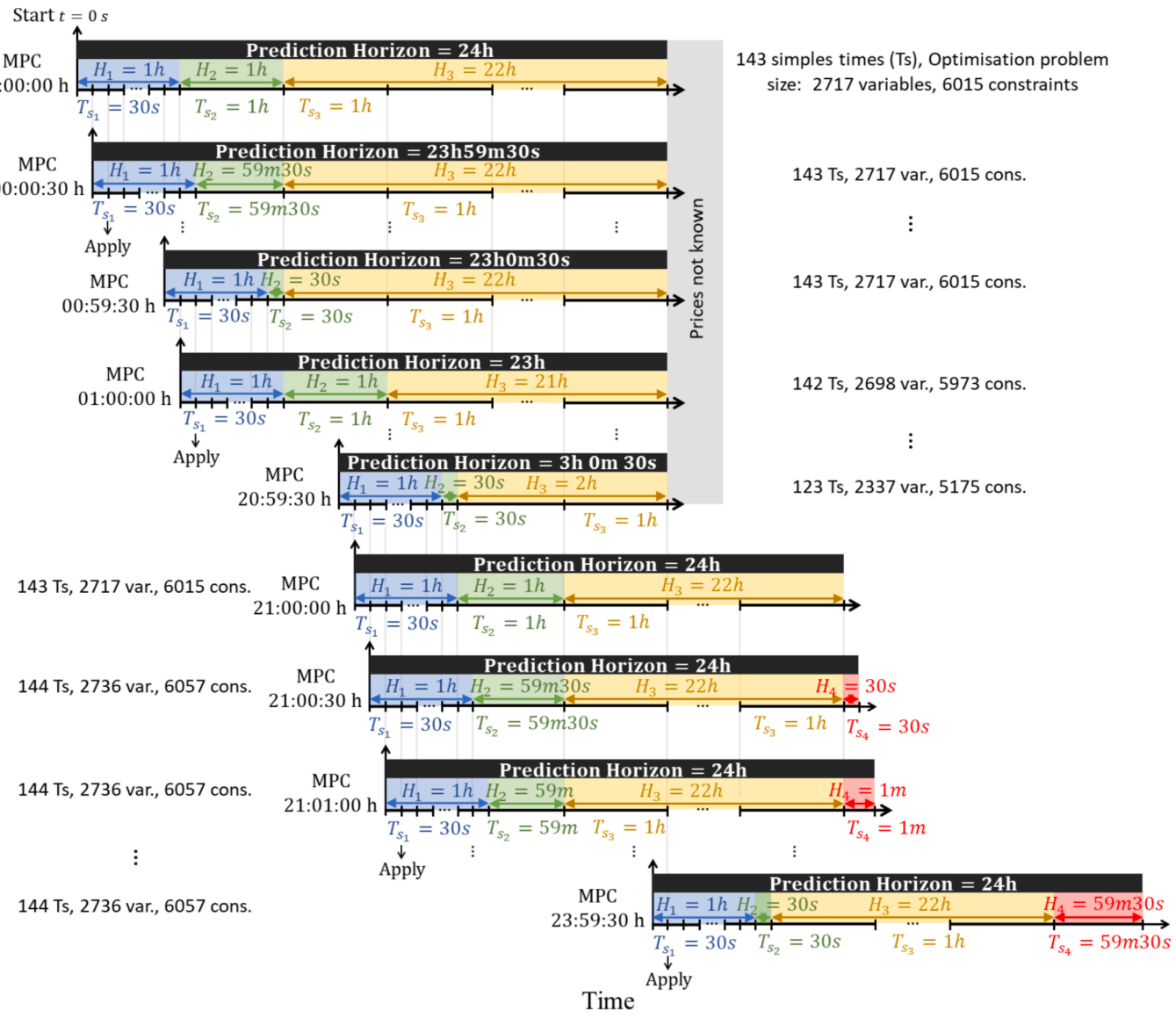

Fig. 4. Control scheme for the first proposed variant (MB-MPC1), detailing its specific move-blocking configuration.

introductory section, the performance of this controller is highly dependent on the appropriate selection of weighting factors. These weights were determined by analysing the individual contribution of each term to the overall cost function, as well as their interdependencies, which reflect the intended operational behaviour of both the HESS and the MEG components within the microgrid. In this study, two different LL control configurations with distinct sets of weights are employed to evaluate performance.

In the first control setting, referred to as BA-MPC1, the weights ω_{Start_i}, $\omega_{\delta P_i}$ and ω_{SOC_j} are set to zero, resulting in a classical power tracking problem. In this setup, only the weights ω_{P_i} are specified for each MEF_i, and all are assigned a unitary value, implying that all power deviations are treated with equal importance. This approach simplifies the controller design by avoiding the need to tune multiple weighting factors.

The BA-MPC1 control setting defines an MPC in the HL comprising between 24 and 4 sampling periods T_s, 18 decision variables per T_S, and between 168 and 968 constraints. On average, this corresponds to 15 T_s, 270 decision variables, and 608 constraints. This simplification of the cost index in the LL controller, due to the zero weights, reduces its complexity by eliminating the $Start_i$, δP_i and Y_i variables. Thus, the LL MPC consists of between 1 and 120 T_S, 13 decision variables per T_S, and between 32 and 2,769 constraints. The average LL configuration includes 60 T_S, 780 decision variables, and 1,389 constraints.

In contrast, the second control setting, referred to as BA-MPC2, employs a more deliberate selection of weights based on the intended roles of the ESS and MEG within the microgrid. The weights are chosen to prioritise the use of the HESS over the MEG, assigning the BSS as the short-term ESS and the HBSS as the long-term ESS. Specifically, the BSS is intended to absorb or supply fast power transients, while the HBSS manages energy over longer periods. The grid serves as a backup to ensure power balance, as defined in Eq. (8). Therefore, the power tracking weights are assigned as follows: $\omega_{P_{ch/dis\_bat}} < \omega_{P_{ch/dis_{H2}}} < \omega_{P_{grid_{s/p}}}$.

Additionally, extra weighting factors are introduced to penalize: (1) deviations in the SOC of the ESS (ω_{SOC_j}), (2) start-up events of the hydrogen-based systems (ω_{Start_i}) and (3) power fluctuations in the hydrogen system ($\omega_{\delta P_i}$). These weights are normalised with respect to the maximum power capacity of each device. In the case of power fluctuation penalties, normalisation is based on the maximum expected fluctuation. The final values, summarised in Table 5, were determined through a trial-and-error procedure, selecting the configurations that minimised the overall cost index.

The BA-MPC2 control setting defines the same HL MPC structure as

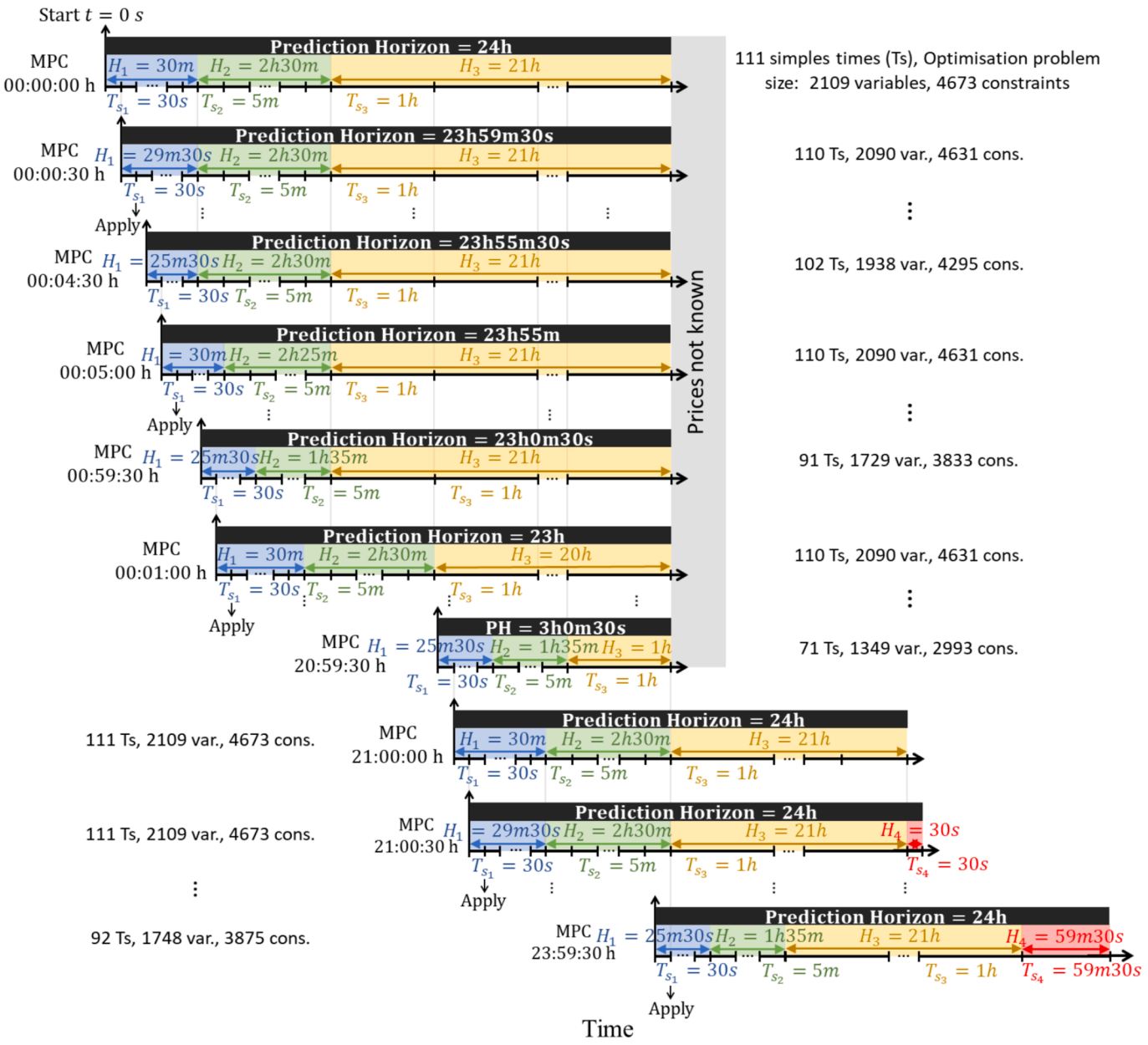

Fig. 5. Control scheme for the second proposed variant (MB-MPC2), detailing its specific move-blocking configuration.

BA-MPC1 (average size: 15 T_S, 270 decision variables, and 608 constraints). However, the LL MPC is not simplified and thus retains higher complexity. It comprises between 1 and 120 T_S, 19 decision variables per T_S, and between 52 and 5,169 constraints. On average, the LL configuration includes 60 T_S, 1,140 decision variables, and 2,589 constraints.

6.2.2. MB-MPC approach

To evaluate the proposed approach, it is essential to assess its overall performance and understand how variations in the number of sampling periods and inner horizons durations affect the behaviour of the MB-MPC method. To this end, this study analyses two variants of the proposed method, each employing a different set of sampling time vectors. While there are numerous possible configurations, the analysis focuses on two representative cases.

The first variant, referred to as MB-MPC1 (see Fig. 4), is designed to align with the structure of the bilevel comparison method, enabling a fair and consistent evaluation between both strategies. This approach solves the optimisation problem described in Eq. (5) every $T_{S_1} = 30sec$. It incorporates two primary sampling periods, T_{S_1} and T_{S_3}, along with one or two supplementary periods, T_{S_2} and T_{S_4}, to ensure accurate alignment with the hourly discretisation of energy prices.

In this configuration, inner horizon H_1 adopts a sampling period $T_{S_1} = 30sec$, identical to the LL controller's sampling period used by the bilevel approach ($T_{S_1} = T_{S_{LL}}$), and spans a 1-hour ($PH_{LL} = H_1 = 1h$). Inner horizon H_3 employs a sampling period $T_{S_3} = 1h$, equivalent to the sampling period of the HL controller ($T_{S_3} = T_{S_{HL}}$). As a result, MB-MPC1 effectively replicates the bilevel control scheme, offering a combined capacity to handle both short-term system dynamics and long-term economic optimisation.

Inner horizon H_2 consists of a single sampling period, $T_{S_2} = H_2$, whose primary role is to ensure that horizon H_3 commences precisely at the start of the next full hour, thus maintaining alignment with the hourly pricing intervals. For instance, a sampling period extending from 21:30 to 22:30 would be misaligned, as energy prices are defined from 21:00 to 22:00 and from 22:00 to 23:00. Therefore, the duration of H_2

(and hence T_{S_2}) is adjusted to fill the gap between the end of H_1 and the beginning of the next full hour, ranging from 30 s to 1 h. Once H_2 reduces to 30 s, it is reset to its original duration of 1 h in the subsequent iteration ($H_2 = 1h$).

At this stage, two scenarios are possible: (1) the energy prices for the following day are not yet available, in which case inner horizon H_3 must be shortened accordingly; or (2) the prices are known, allowing H_3 to maintain its original duration, with the addition of a new inner horizon H_4 that employs a single sampling is period T_{S_4} until $HP = 24h$. is reached. This iterative process continues until the 24-hour duration of the scenario is reached.

As can be seen in Fig. 4, this variant initially defines an MPC comprising 143 sampling periods T_S (120 in H_1, 1 in H_2, and 22 in H_3). Each sampling period involves 19 decision variables (as detailed in Table 1), resulting in an initial optimisation problem with 2,717 decision variables and 6,015 constraints, comprising 575 equality constraints (related to SOC_j, V_{BUS}, and power balance) and 5,440 inequality constraints. In this variant, the MPC size can be reduced to 123 T_S, with 2,337 decision variables and 5,175 constraints (at 20:59:30 h). On average, this variant operates with 134 T_S, 2,546 decision variables, and 5,637 constraints.

The second variant, referred to as MB-MPC2 (see Fig. 5), initially applies the same optimisation problem as the first variant but incorporates a new sampling period (T_{S_2}), specifically designed to better capture the typical dynamics of generation and demand profiles and the behaviour of the HESS.

As in MB-MPC1, the first sampling period is set to$T_{S_1} = T_{S_{LL}}$ and is applied over an initial inner horizon of 30 min (H_1). A second sampling period $T_{S_2} = 5$ min, is used over an additional 2.5-hour inner horizon (H_2). This configuration enables the controller to finely adjust the response of both the HESS and MEG to short-term fluctuations in generation and demand, while adequately addressing the slower dynamics of the HBSS. Lastly, to incorporate long-term optimisation, a third sampling period $T_{S_3} = T_{S_{HL}}$ is applied over a 21-hour time inner horizon (H_3), completing the 24-hour PH. Additionally, when energy prices for the following day are known and trimming is not required, a fourth inner horizon (H_4) with a single sampling period T_{S_4} is included to maintain $PH = 24h$.

Throughout the control process, the duration of H_1 is iteratively reduced by T_{S_1}, in each step, until it reaches 25:30 min. Then, in the next iteration, H_1 returns to its original duration of 30 min. This cyclical adjustment ensures that an hourly change never occurs withing sampling period in H_2. For instance, a sampling time in H_2 from 00:55:30 h to 01:00:30 h would be problematic, as it would be unclear whether to apply the electricity price from 00 h to 01 h or from 01 h to 02 h.

Once H_1 returns to its original size, H_2 is shortened by $T_{S_2} = 5$ min. This process is repeated, trimming H_1 until it reaches 25 min and 30 s, then reducing H_2 in the next iteration, until the start of the optimisation aligns precisely with the beginning of an hour. At this point, the original durations are reinstated ($H_1 = 30$ min and $H_2 = 2$ h and 30 min). As a result, the duration of H_2 fluctuates between within 1:35 to 2:30 h, ensuring that H_3 always begins exactly at the start of an hour, similar to the approach adopted in MB-MPC1.

At this point, if the energy prices for the following day are not yet available, H_3 is trimmed by $T_{S_3} = 1h$. Otherwise, H_3 maintains its original size ($H_3 = 21h$), and the additional horizon H_4 with sampling period T_{S_4} is introduced to maintain the full 24-hour PH. This iterative process continues until the 24-hour duration of the scenario is reached.

Initially, this variant defines an MPC comprising 111 sampling periods T_S (60 in H_1, 30 in H_2, and 21 in H_3). Each sampling period involves 19 decision variables (see Table 1), resulting in a total of 2,109 decision variables and 4,673 constraints, comprising 447 equality constraints (accounting for SOC_j, V_{BUS}, and power balance) and 4,226 inequalities. In this variant, the size of the MPC can be reduced to 71 T_s, with 1,349 decision variables and 2,993 constraints (at 20:59:30 h). On average, MB-MPC2 operates with 92 T_s, 1,748 decision variables, and 3,875 constraints.

6.3. Results

The objective of this study is to validate the performance of the proposed EMS in terms of system behaviour, economic efficiency, and computational cost, by comparing it with the most computationally feasible EMS solutions commonly used in the scientific literature. To this end, this section presents the results obtained for two variants of the MPC-based EMS under investigation: MB-MPC1 and MB-MPC2 (the novel approach introduced in this work), and two different controller settings of the bilevel approach (BA-MPC1 and BA-MPC2) based on references [17] and [21]. All are compared against a single-level optimal MPC-based EMS, which serves as the reference response.

Specifically, the assessment of computational feasibility considers the average computation time per iteration for each approach and variant. To further demonstrate their applicability in real-time scenarios, a timeout threshold equal to $T_{S_{LL}}$ has been imposed. If the solver fails to obtain an optimal solution within this period, the process is interrupted, and the best available sub-optimal control vector is applied. This ensures continuity in the control process and enables a realistic assessment of each method's feasibility. The number of such interruptions is also reported as an indicator of computational robustness.

The economic analysis focuses on total operating costs and the de-

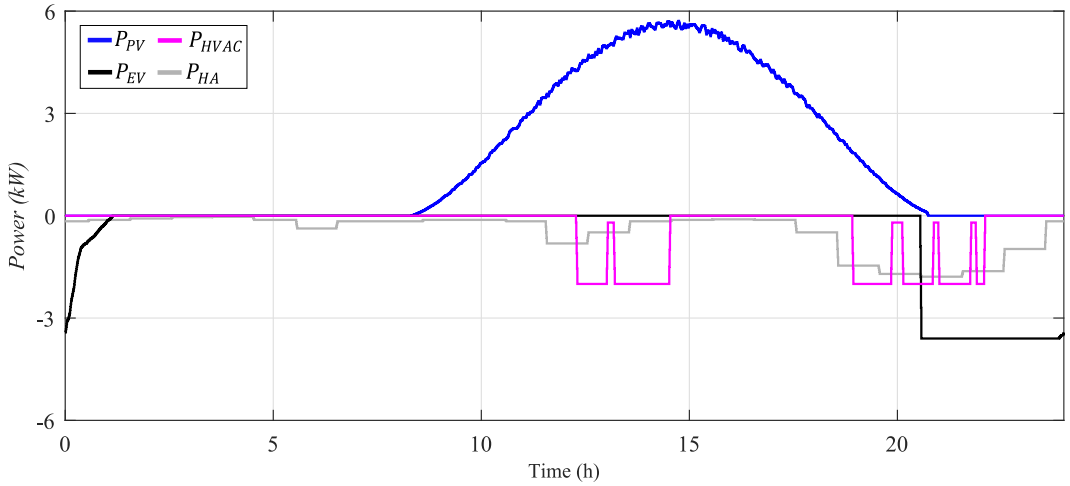

Fig. 6. Daily profiles for photovoltaic generation (P_{PV}) and aggregated residential loads ($P_{Load} = P_{HVAC} + P_{HA} + P_{EV}$) used as the baseline scenario for all simulations.

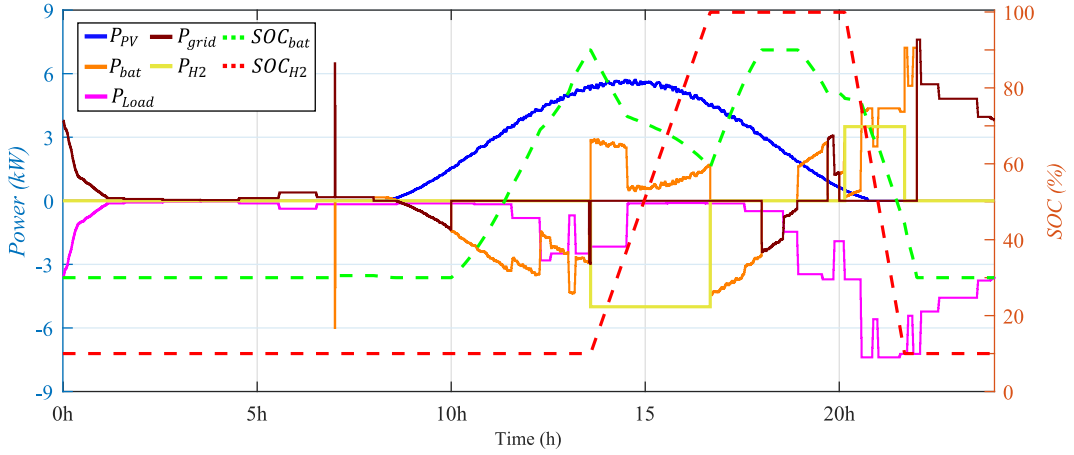

Fig. 7. Power and SOC profiles for the optimal MPC-based EMS, serving as the ideal performance benchmark under the defined residential scenario.

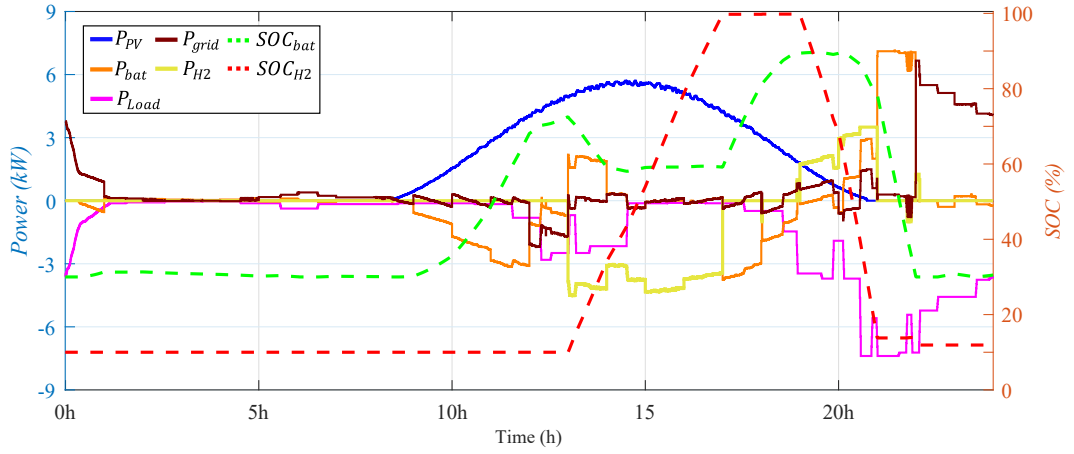

Fig. 8. Power and SOC profiles for the BA-MPC1 (bi-level approach and control setting 1) under the defined residential scenario.

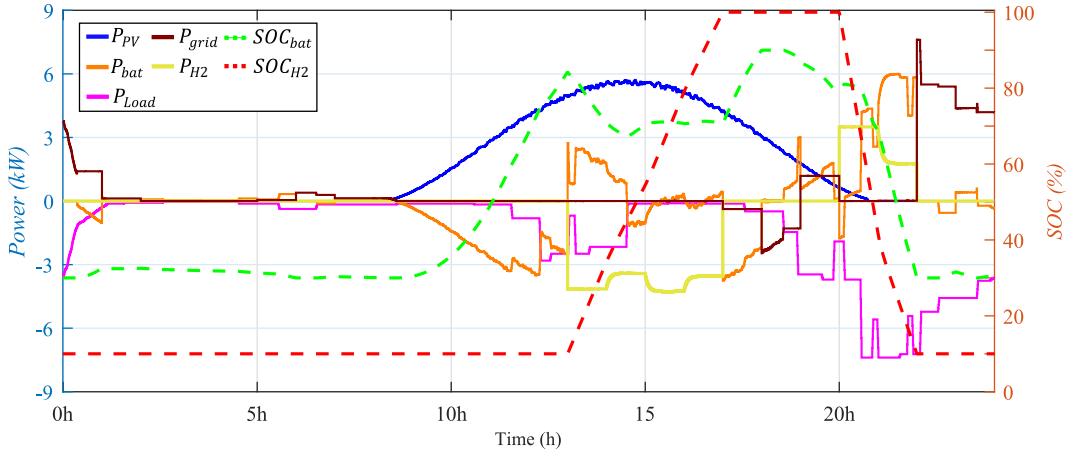

Fig. 9. Power and SOC profiles for the BA-MPC2 (bi-level approach and control setting 2) under the defined residential scenario.

viation from the economically optimal reference case. For this purpose, the responses of all EMS configurations and variants are compared against the "reference response" provided by a single-level economic MPC-based EMS. This reference controller is configured with a PH equivalent to that of the HL controller ($PH = PH_{HL}$) and a sampling period equal to that of the LL controller ($T_S = T_{S_{LL}}$). Although this setup provides the most economically optimal solution, its high computational burden renders it unsuitable for real-time application. Therefore, it is used solely as a reference response to assess the relative performance of the proposed methods.

All simulations follow the optimisation methodology described in [8], with design parameters, cost structures, constraints, system losses, models, decision variables, and the optimisation index aligned with those adopted for the proposed method (see Section 5).

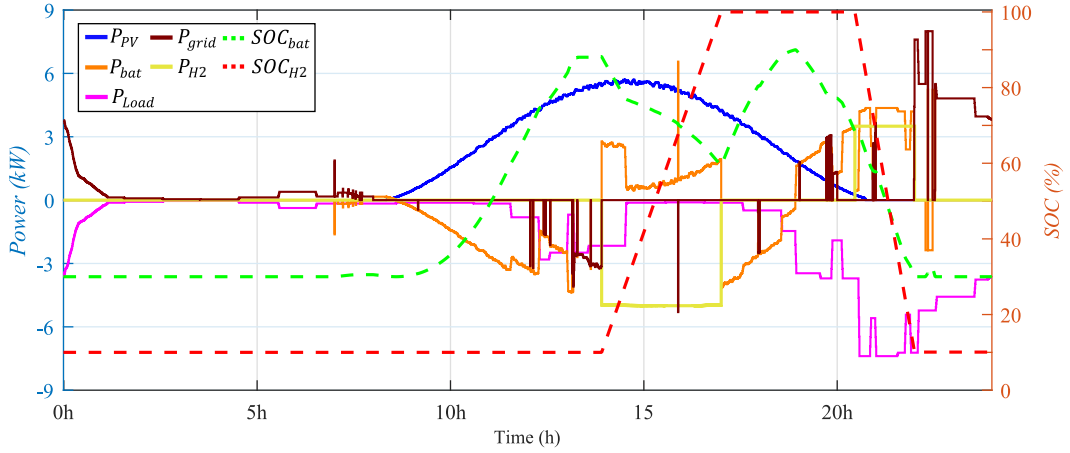

Fig. 10. Power and SOC profiles for the MB-MPC1 (move-blocking approach, variant 1) under the defined residential scenario.

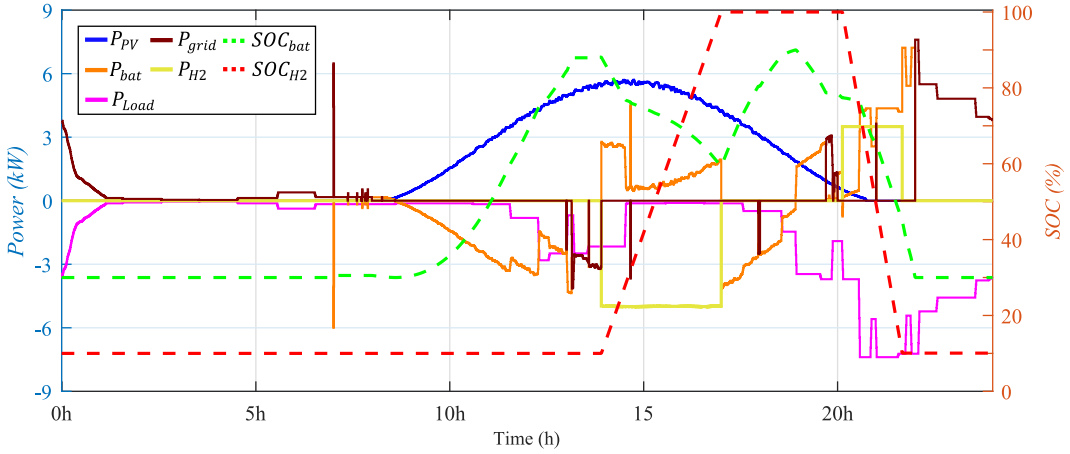

Fig. 11. Power and SOC profiles for the MB-MPC2 (move-blocking approach, variant 2) under the defined residential scenario.

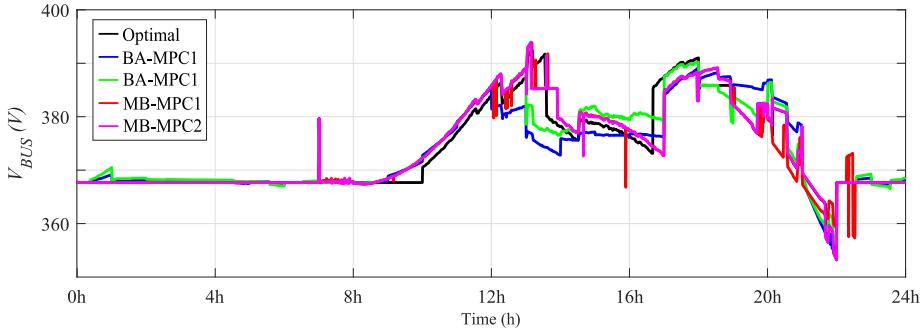

Fig. 12. Comparison of V_{BUS} regulation across all evaluated strategies under the defined residential scenario.

In the scenario under study, all approaches are evaluated under the same conditions, including identical renewable generation (P_{PV}) and demand profiles (P_{Load}), as well as the same initial conditions for the state vector: $V_{BUS}(0) = 367.75V$, $SOC_{bat}(0) = 30$ %, $SOC_{H2}(0) = 10$ %. Fig. 6 presents the renewable generation and load profiles used in the evaluated scenario. The total load power (P_{Load}) consists of heating, ventilation and air conditioning (P_{HVAC}), electric vehicle (P_{EV}), and household appliance (P_{HA}) power ($P_{Load} = P_{HVAC} + P_{HA} + P_{EV}$).

Both P_{PV} and P_{Load} are shown in the results, along with the power outputs and state of charge (SOC) profiles obtained for each analysed approach. For this study, a low energy profile was selected for the HESS to increase flexibility in managing energy surpluses and deficits.

Regarding the results, Figs. 7-12 present the simulation outcomes derived from the case study based on the microgrid architecture depicted in Fig. 1. Specifically, Figs. 8 and 9 depict the power flows and SOC profiles (SOC_{bat} and SOC_{H2}) for the bilevel approaches. Figs. 10 and 11 display the corresponding results for the MB-MPC1 and MB-MPC2 approaches, respectively. Given the microgrid architecture (Fig. 1), maintaining the DC bus voltage (V_{BUS}) within the allowable range is crucial for system stability. Accordingly, Fig. 12 illustrates the V_{BUS} profile for all approaches through the simulation period.

Finally, Table 7 summarises the economic cost breakdown relative to

Table 6
Comparison of final economic costs (€) by each approach.

MPC-based EMS	Total variable cost* C^{var}(€)	Total fix cost* C^{fix}(€)	Total start cost* C^{Start}(€)	Total degradation cost* C^{deg}(€)	Total Cost (€)
Optimal	0.971	0.090	0.1	0	1.160
BA-MPC1	1.145	0.120	0.4	0.0245	1.690
BA-MPC2	1.048	0.116	0.1	0.0015	1.265
MB-MPC1	0.974	0.090	0.1	0	1.164
MB-MPC2	0.972	0.090	0.1	0	1.161

* $C^{var} = \sum_k \sum_i C_i^{var}(k) \cdot P_i(k), C^{fix} = \sum_k \sum_i C_i^{fix}(k) \cdot WT_i(k)$, $C^{Start} = \sum_k \sum_i C_i^{Start}(k) \cdot Start_i(k)$ and $C^{deg} = \sum_k \sum_i C_i^{deg}(k) \cdot \delta P_i^2(k)$.

Table 7
Comparison of computational costs obtained by each approach.

MPC-based EMS		Average size of the optimisation problem			Time out events	Computational Cost** (sec.)
		T_s	Decision Variables	Constraints		
Optimal		2880	54,720	123,849	0	831
BA-MPC1	HL	15	270	608	386	6.87
	LL	60	780	1,389		
BA-MPC2	HL	15	270	608	48	1.56
	LL	60	1,140	2,589		
MB-MPC1		134	2,546	5,175	0	2.24
MB-MPC2		92	1,748	3,875	0	1.67

the reference case, along with the average computational time per iteration, providing a comprehensive comparison across all evaluated EMS strategies.

6.4. Discussion

The performance of the microgrid is first evaluated using a reference EMS. Fig. 7 presents the results obtained with this optimal MPC-based approach. In this analysis, positive power values indicate energy supplied to the bus (e.g., battery discharge $P_{dis_{bat}}$, hydrogen consumption $P_{dis_{H2}}$, and grid purchase P_{grid_p}), while negative values denote power consumed from the bus (e.g., battery charge $P_{ch_{bat}}$, hydrogen production $P_{ch_{H2}}$, and grid sale P_{grid_s}).

The simulation begins at midnight, during which the EV reaches full charge within the first hour. At 07 h, a peak in grid power purchase occurs, partially charging the battery and avoiding higher-cost purchases during the 08:00–08:30 interval, as detailed in Table 4. PV generation starts at sunrise, covering household demand and simultaneously charging the ESS. However, more energy is generated than can be stored in the ESS ($\overline{SOC_{bat}} = 90\%$ and $\overline{SOC_{H2}} = 100\%$). Therefore, any excess energy is exported to the MEG, resulting in financial profit or loss depending on sale prices.

Towards evening, an energy deficit emerges. The system minimises grid purchases during the high-price window of 19 h–22 h, by relying on stored ESS energy (see purchase price in Table 4). A single purchase is made between 19:45 and 20:00 due to insufficient stored energy. Notably, the electrolyser and fuel cell operate at constant power to mitigate degradation costs, running at maximum capacity to reduce activation time and fixed costs.

Economic and computation metrics for this approach are summarised in Tables 6 and 7. The total operational cost is €1.16, predominantly from variable energy costs. However, the computation time exceeds thirteen minutes per iteration, rendering the approach infeasible for real-time applications, given the 30-second sampling time ($T_{S_{LL}} = 30sec$). The optimal MPC comprises 2,880 sampling periods T_S, 54,720 decision variables, and 123,849 constraints (11,523 equality and 112,326 inequality constraints).

Next, the performance of the bilevel EMS tracking approach is examined for the two previously defined controller configurations (Section 6.1.2). Fig. 8 presents the results for Controller Configuration 1 (BA-MPC1), which employs normalised unitary weights (as specified in Table 5) to penalise deviations from reference power trajectories (P_i^{ref}). This methodology eliminates the need for explicit weight definition in the lower-level (LL) optimisation index.

During daylight operation, the system repeatedly cycles between purchasing and selling energy to the MEG, even in the presence of surplus renewable generation. This behaviour proves economically suboptimal, as the cost of purchased power exceeds the revenue from power sales, resulting in unfavourable economic outcomes. The root cause lies in the LL controller's rigid adherence to the reference power commands. For instance, at 09 h, the HL controller specifies a battery charging reference of $P_{ch_{bat}}^{ref} = 836.7$ W (with all other power references set to zero), intending to utilize excess solar generation for battery charging. However, actual PV output initially falls below predicted levels, prompting the MPC to purchase grid power to maintain alignment with the charging reference. As PV generation later exceeds forecasts, the system sells surplus energy to the grid to continue tracking the reference. This cyclical pattern persists throughout morning hours, contributing to cumulative economic losses.

Additionally, the system exhibits variable operation of the HBSS and excessive cycling of the electrolyser. For example, during the 21 h-22 h period, while the HL controller specifies battery discharge as the sole active power flow ($P_{dis_{bat}} = 6982.7$ W, with other references at zero), significant load fluctuations occur. The initial load demand ($P_{Load} = 7387.5$ W) substantially exceeds the subsequent demand ($P_{Load} = 2425$ W) due to reduced HVAC consumption. To minimise deviation from the power reference, the LL controller activates the electrolyser, which features a minimum operating power of $P_{ch_{H2}} = 1000$ W and associated BoP losses ($Loss_i^{BoP} = 1000$ W). Given these losses, it is more effective at deviation minimisation than devices without such characteristics. For instance, when excess power reaches 2000 W, the electrolyser's effective deviation is only 1000 W ($P_{ch_{H2}} = 1000$ W), given its 1000 W BoP losses, whereas non-BoP devices would register the full 2000 W deviation. This operational characteristic explains the observed frequent electrolyser activation between 21 h and 22 h.

Consequently, this control approach exhibits two significant drawbacks: (1) persistent and economically inefficient grid trading, and (2) unnecessary cycling of the HBSS. These effects are quantified in Tables 6 and 7, which show a 45 % increase in total operational costs relative to the optimal EMS. Nonetheless, the computational cost is reduced by 98 %, making this approach suitable for real-time deployment. Despite all power flows and SOC values remaining within the limits defined in Table 2, this controller configuration encountered timeout events in 386 iterations.

Fig. 9 demonstrates the operational characteristics of Controller Configuration 2 (BA-MPC2), which incorporates the weighting scheme from Table 5. This configuration exhibits substantial improvements over BA-MPC1, achieving optimal utilisation of the MEG through complete elimination of unnecessary energy transactions. This enhancement is primarily attributed to the application of higher penalty coefficients for deviations in MEG power, which effectively discourages unprofitable transactions and reduces variable costs by minimising MEG energy purchases. The system also demonstrated improved operational stability of the HBSS. The introduction of start-up penalties (ω_{Start_i}) successfully curtails frequent electrolyser cycling, promoting steady-state operation and thereby mitigating power fluctuations and the associated degradation costs.

The enhanced control methodology effectively mitigates the two principal limitations identified in BA-MPC1 operation: persistent and

economically inefficient energy trading with the MEG, and excessive cycling of HBSS components. As shown in Tables 6 and 7, this optimised configuration restricts the increase in total operational cost to only 9 % relative to the optimal EMS, representing a considerable improvement over the 45 % cost escalation recorded for BA-MPC1. Furthermore, it achieves a 77 % reduction in computational time compared to the BA-MPC1 configuration.

Despite maintaining strict adherence to all power and SOC boundaries defined in Table 2, the optimisation process encounters 48 timeout occurrences with this controller setting. These findings underscore the potential of carefully tuned penalty coefficients in bi-level control architectures to deliver significant economic and operational benefits. However, the approach's effectiveness remains intrinsically dependent on the proper selection of these parameters. Notably, the weights must be tailored not only to the specific microgrid architecture but also to the operational context, such as weather conditions (e.g. cloudy, sunny, or winter days) as highlighted in [30].

The performance of the novel approach proposed in this work is analysed below. Specifically, Fig. 10 illustrates the results obtained for variant 1 (MB-MPC1, see Section 6.1.2), which was designed to follow a similar philosophy to that of the previously discussed bi-level approach. As observed, this variant yields a system response that more closely approximates the optimal MPC-based strategy compared to the bi-level methods. Notably, it successfully avoids purchasing energy during the 8:00–8:30 interval by procuring it earlier at a lower cost and storing it in the BSS, thereby emulating the optimal MPC's operational decisions.

Additionally, the hydrogen-based devices operate at maximum power during their entire active period, minimising power fluctuations and reducing the total operation time. This operational mode decreases BoP losses and substantially reduces the energy purchased from the MEG during the 19 h–22 h interval, as depicted in Fig. 10.

These improvements contribute to lower variable (C^{var}), fixed (C^{fix}), and degradation (C^{deg}) costs compared to the bi-level approach (see Table 6). As a result, the total cost incurred by MB-MPC1 is only 0.8 % higher than that of the optimal approach and 8 % lower than that of BA-MPC2, demonstrating near-optimal economic performance. Furthermore, the optimiser never reaches the timeout limit, achieving a computation time that is 99 % lower than the reference approach and only marginally higher than that of BA-MPC2 (see Table 7), thereby confirming the feasibility of this strategy for real-time applications.

On the other hand, Fig. 11 presents the results for variant 2 (MB-MPC2, see Section 6.1.2), which exhibits performance similar to that of MB-MPC1. Once again, the hydrogen devices are operated at full capacity, effectively reducing power variability and limiting their active periods. This configuration also decreases the reliance on MEG energy purchases when compared to the bi-level approaches.

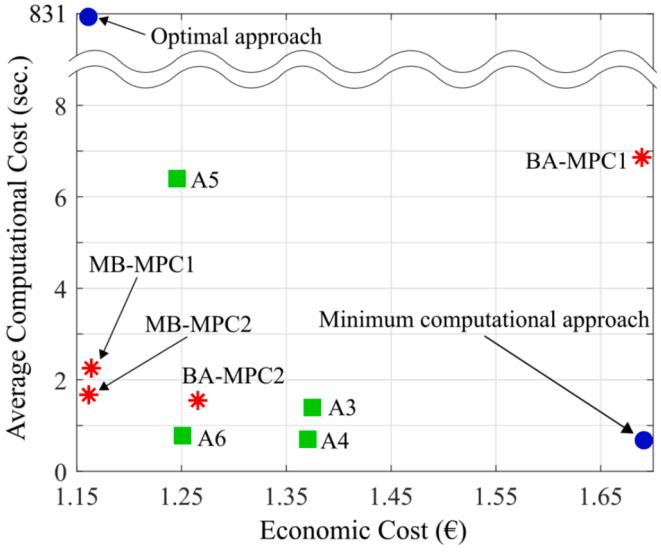

Fig. 13. Trade-off analysis comparing the final economic cost (€) and the average computational time per iteration (s) for each evaluated control approach.

The cost metrics for MB-MPC2 are nearly identical to those of MB-MPC1 (see Table 6), with a marginally lower variable cost (C^{var}). As a result, the total cost is only 0.3 % higher than of the optimal MPC solution, reaffirming the approach's close alignment with reference performance. In this configuration, the optimiser does not encounter any timeout events, and the computational cost is comparable to that of BA-MPC2, while remaining 99 % lower than that of the reference case (see Table 7).

Next, given the architecture of the microgrid under study, it is important to evaluate the behaviour of the state variable V_{BUS}. As shown in Fig. 12, regardless of the control approach, and despite instantaneous fluctuations in DC bus power, V_{BUS} consistently remains within the limits established by the control problem constraints (330–450 V). This confirms that the MPC approach is effective and reliable for managing microgrids of this type.

The results across all scenarios reveal two notable limitations of the MPC tracking approach: (1) persistent energy trading with the MEG, and (2) unnecessary operation cycles of the electrolyser and fuel cell, both of which increase operational costs. Although careful weight selection can mitigate these issues, the process introduces its own challenges: weight definition is inherently complex and often requires trial-and-error procedures that frequently lead to suboptimal solutions. Moreover, these weights are scenario-specific and dependent on the microgrid architecture, thereby limiting the generalisability of the solution.

In contrast, the proposed new approach eliminates these undesirable effects, removes the need for trial-and-error weight selection, and consistently delivers better economic outcomes than the tracking approach. Additionally, it enhances HBSS management, resulting in a stable power profile for the electrolyser and fuel cell. This reduces the total degradation cost ($C^{deg} = \sum_k \sum_i C_i^{deg}(k) \cdot \delta P_i^2(k)$). Moreover, HBSS operates consistently at full power, minimising operating time and thereby lowering the total fixed cost ($C^{fix} = \sum_k \sum_i C_i^{fix}(k) \cdot WT_i(k)$). This efficient operational strategy also decreases reliance on MEG energy purchases, contributing to lower variable costs ($C^{var} = \sum_k \sum_i C_i^{var}(k) \cdot P_i(k)$.

Regarding computational performance, both the bi-level and proposed approaches exhibit acceptable average computation times per iteration (Table 7). The bi-level approach defines two simpler MPCs per iteration. For instance, BA-MPC2 defines two MPCs of 270 and 1140 variables, and 608 and 2589 constraints, respectively, resulting in an average computational cost of 1.56 s per iteration. The proposed approach defines a single, slightly more complex MPC. As an example, MB-MPC2 yields an average MPC formulation comprising 1748 variables and 3875 constraints. Despite this greater complexity, it remains computationally affordable, with an average computational cost of 1.67 s per iteration. Furthermore, unlike the bilevel approach experienced timeout events (386 instances with BA-MPC1 and 48 with BA-MPC2), the proposed method consistently completes within the allotted time.

The findings from the case study demonstrate that, although MB-MPC shares certain limitations inherent to computationally efficient advanced MPC strategies, such as suboptimality, increased reliance on accurate system modelling, and the need for supervisory oversight, it offers clear advantages over the conventional bilevel hierarchical EMS. Specifically, the proposed framework substantially reduces computational complexity, eliminates the necessity for inter-layer coordination, and enhances real-time applicability through its unified single-level structure. Moreover, by adopting an economic objective function, it obviates the need for manual weight tuning, which is often required in multi-objective formulations.

Collectively, these attributes position the MB-MPC framework as a

robust, scalable, and practically viable control solution for managing the multi-temporal dynamics characteristic of microgrid systems, particularly in scenarios where both operational efficiency and implementation simplicity are critical.

6.4.1. Evaluation of move-blocking sampling strategies

To validate the selection of horizons and sampling periods for the move-blocking approach, a posteriori sensitivity analysis was conducted (see Fig. 13). The analysis evaluates the trade-off between two main objectives: economic and computational cost**. Each configuration optimises an MPC every 30 s with a 24-hour prediction horizon (HP), following the methodology described in Section 6.2.2.

To establish the limits of the analysis, two extreme approaches are compared:

- Optimal approach (Section 6.3): A single optimisation with a fine and constant sampling period ($T_S = 30s$). It achieves the minimum economic cost (€1.16) but with an unfeasible computational cost (831 sec.) for real-time operation.
- Minimum computational approach: A configuration with a large and constant sampling period ($T_S = 1h$), analogous to the MB-MPC1 variant with $T_{S1} = 1h$. It offers the lowest computational cost but the worst economic result (€1.69). It should be noted that this approach achieves a similar economic cost, with significantly lower computational costs, than the bilevel approach BA-MPC1 (Section 6.3).

Furthermore, different alternative move-blocking configurations based on the MB-MPC1 variant were evaluated, varying the main sampling periods (T_{S1}, for the short-term, and T_{S3}, for the long-term). T_{S2} and T_{S4} are only used to ensure accurate alignment with the hourly discretization of energy prices. The results are summarised below:

- Approach A3, $T_{S_1} = 15min.$ and $T_{S_3} = 15min.$: the economic cost is €1.37 and the computational cost is 1.37 s.
- Approach A4, $T_{S_1} = 15min.$ and $T_{S_3} = 1h.$: the economic cost remains at €1.37, but the computational cost is reduced to 0.7 s.
- Approach A5, $T_{S_1} = 5min.$ and $T_{S_3} = 5min.$: the economic cost improves to €1.25, with a computational cost of 6.4 s.
- Approach A6, $T_{S_1} = 5min.$ and $T_{S_3} = 1h.$: the economic cost is €1.25 and the computational cost is drastically reduced to 0.8 s. This result is comparable in economic cost to the BA-MPC2 approach but with a lower computational cost.

The results shows two clear patterns:

- Impact of T_{S_3}: Increasing the sampling period for distant horizons drastically reduces the computational cost without penalizing the economic result.
- Impact of T_{S_1}: Reducing the sampling period for the near horizon notably improves the economic cost, although it increases the computation time.

Fig. 13 illustrates that the two move-blocking variants defined in this work (MB-MPC1 and MB-MPC2) achieve a near-optimal economic cost with a computational cost suitable for real-time implementation. This outcome validates that a move-blocking approach is a highly efficient strategy. Employing a short sampling period for the near horizon and a longer one for the far horizon provides an excellent trade-off, yielding strong economic performance while significantly reducing the computational burden. While this analysis validates the two variants proposed, the possibility that other move-blocking configurations could offer further slight improvements is not ruled out.

7. Conclusions

This paper has presented and validated an innovative single-layer, move-blocking MPC-based EMS for complex renewable microgrids. The proposed framework successfully integrates multi-time scale objectives into a unified economic optimisation model, eliminating the need for complex hierarchical architectures and the manual tuning of weighting factors.

The performance evaluation demonstrated significant quantitative improvements. The proposed EMS reduced total operating costs by over 8 %. This saving is composed of three key factors: a 13 % decrease in degradation-related costs attributable to more stable HESS management, a reduction in fixed operating costs by minimising the usage time of the hydrogen systems, and a 7 % reduction in variable energy costs. Computationally, the strategy proved highly efficient, reducing computation time by 99 % compared to an optimal reference case while achieving performance comparable to the benchmarked bilevel approach, confirming its real-time feasibility.

These findings have significant implications for the development of simpler, scalable, and economically efficient EMS solutions. The move-blocking approach is confirmed as a robust strategy for achieving high performance in real-time applications without relying on complex, multi-layer control structures. Despite these promising results, it is acknowledged that this validation was limited to a specific microgrid architecture. Further sensitivity analysis would be beneficial to generalise the findings and identify optimal configurations for a broader range of operating conditions and microgrid topologies.

Future research will focus on extending the framework to more complex microgrid configurations and integrating uncertainty from forecasts and disturbances. Long-term, annual-basis evaluations will also be explored to further assess its applicability in real-world scenarios.

CRediT authorship contribution statement

A. Pajares: Writing – original draft, Software, Methodology, Investigation, Conceptualization. **F.J. Vivas:** Writing – original draft, Methodology, Investigation, Conceptualization. **X. Blasco:** Writing – review & editing, Validation, Supervision, Project administration, Investigation. **J.M. Herrero:** Writing – review & editing, Validation, Supervision, Project administration, Investigation. **F. Segura:** Writing – review & editing, Supervision, Project administration. **J.M. Andújar:** Writing – review & editing, Supervision, Project administration, Investigation, Funding acquisition.

Declaration of competing interest

The authors declare that they have no known competing financial interests or personal relationships that could have appeared to influence the work reported in this paper.

Acknowledgements

This work has been funded by project PID2023-148456OB-C41 and PID2021-124908NB-I00, funded by MICIU/AEI/10.13039/501100011033 and by "ERDF A way of making Europe".

Data availability

Data will be made available on request.

References

[1] Vivas FJ, De las Heras A, Segura F, Andújar JM. A review of energy management strategies for renewable hybrid energy systems with hydrogen backup. Renew Sustainable Energy Rev 2018;82.

[2] Kumar J, Agarwal A, Agarwal V. A review on overall control of DC microgrids. J Energy Storage 2019;21(November 2018):113–38.
[3] Papadimitriou CN, Zountouridou EI, Hatziargyriou ND. Review of hierarchical control in DC microgrids. Electr Pow Syst Res 2015;122:159–67.
[4] Hajiaghasi S, Salemnia A, Hamzeh M. Hybrid energy storage system for microgrids applications: A review. J Energy Storage 2019;21(November 2018):543–70.
[5] Vivas FJ, Segura F, Andújar JM, Caparrós JJ. A suitable state-space model for renewable source-based microgrids with hydrogen as backup for the design of energy management systems. Energ Conver Manage 2020;219:113053.
[6] Vivas FJ, Segura F, Andújar JM. Fuzzy logic-based energy management system for grid-connected residential DC microgrids with multi-stack fuel cell systems: a multi-objective approach. Sustainable Energy Grids Networks 2022;32:100909.
[7] Chen J, Yang P, Peng J, Huang Y, Chen Y, Zeng Z. An improved multi-timescale coordinated control strategy for stand-alone microgrid with hybrid energy storage system. Energies 2018;11(8).
[8] Rose M, Hans CA, Schiffer J. A predictive operation controller for an electro-thermal microgrid utilizing variable flow temperatures. IFAC-PapersOnLine 2023;56(2):5444–50.
[9] Vivas FJ, et al. Multi-objective fuzzy logic-based energy management system for microgrids with battery and hydrogen energy storage system. Electronics (Switzerland) 2020;9(7):1–25.
[10] El Bakali S, Ouadi H, Gheouany S. Efficient real-time cost optimization of a two-layer electric water heater system under model uncertainties. Energ Conver Manage 2024;304(January):118190.
[11] Pajares A, Vivas FJ, Blasco X, Herrero JM, Segura F, Andújar JM. Methodology for energy management strategies design based on predictive control techniques for smart grids. Appl Energy 2023;351(August):121809.
[12] Freire VA, de Arruda LVR, Bordons C, Marquez JJ. Optimal demand response management of a residential microgrid using model predictive control. IEEE Access 2020;8.
[13] Garcia-Torres F, Zafra-Cabeza A, Silva C, Grieu S, Darure T, Estanqueiro A. Model predictive control for microgrid functionalities: review and future challenges. Energies 2021;14(5):1296,.
[14] Hu J, Shan Y, Guerrero JM, Ioinovici A, Chan KW, Rodriguez J. Model predictive control of microgrids – an overview. Renew Sustain Energy Rev Feb. 2021;136:110422.
[15] Hou J, Yu W, Xu Z, Ge Q, Li Z, Meng Y. Multi-time scale optimization scheduling of microgrid considering source and load uncertainty. Electr Pow Syst Res 2023;216(October 2022):109037.
[16] He Y, Li Z, Zhang J, Shi G, Cao W. Day-ahead and intraday multi-time scale microgrid scheduling based on light robustness and MPC. Int J Electr Power Energy Systems 2023;144(July 2022).
[17] Liu C, Wang C, Yin Y, Yang P, Jiang H. Bi-level dispatch and control strategy based on model predictive control for community integrated energy system considering dynamic response performance. Appl Energy 2022;310(December 2021):118641.
[18] Huang C, et al. Economic and resilient operation of hydrogen-based microgrids: an improved MPC-based optimal scheduling scheme considering security constraints of hydrogen facilities. Appl Energy 2023;335(January):120762.
[19] Zhang J, et al. Multi-time scale economic scheduling method based on day-ahead robust optimization and intraday MPC rolling optimization for microgrid. IEEE Access 2021;9:140315–24.
[20] Garcia-Torres F, Bordons C, Tobajas J, Real-Calvo R, Santiago I, Grieu S. Stochastic optimization of microgrids with hybrid energy storage systems for grid flexibility services considering energy forecast uncertainties. IEEE Trans Power Syst 2021;36(6):5537–47.
[21] Hu Q, et al. A spatial data-driven vehicle speed prediction framework for energy management of hevs using multi-horizon MPC with non-uniform sampling. Proceed Am Control Conf 2022;2022-June:1024–9.
[22] Lu Z, Mou S. Variable sampling MPC via differentiable time-warping function. Proceed Am Control Conf 2023;2023-May:533–8.
[23] Yassuda Yamashita D, Vechiu I, Gaubert JP. Two-level hierarchical model predictive control with an optimised cost function for energy management in building microgrids. Appl Energy 2021;285(December 2020).
[24] Yang H, Pu Y, Qiu Y, Li Q, Chen W. Multi-Time Scale Integration of Robust Optimization with MPC for Islanded Hydrogen-based Microgrid. In: iSPEC 2019–2019 IEEE Sustainable Power and Energy Conference: Grid Modernization for Energy Revolution; 2019. p. 1163–8.
[25] Kaya O, Van Der Roest E, Vries D, Keviczky T. Hierarchical model predictive control for energy management of power-to-X systems. In: IEEE PES innovative Smart Grid Technologies Conference Europe; 2020. p. 1094–8.
[26] Lei X, Huang T, Yang Y, Fang Y, Wang P. A bi-layer multi-time coordination method for optimal generation and reserve schedule and dispatch of a grid-connected microgrid. IEEE Access 2019;7:44010–20.
[27] Abdelghany MB, Mariani V, Liuzza D, Glielmo L. Hierarchical model predictive control for islanded and grid-connected microgrids with wind generation and hydrogen energy storage systems. Int J Hydrogen Energy 2024;51:595–610.
[28] Guo X, Gu F, Liu H, Yu Y, Li R, Wang J. Sustainable PV-hydrogen-storage microgrid energy management using a hierarchical economic model predictive control framework. 2025; vol. 8(1).
[29] Pan T, Hou J, Jin X, Yu Z, Zhou W, Wang Z. Distributed control of hydrogen-based microgrids for the demand side: a multiagent self-triggered MPC-based strategy. Algorithms 2024;17(6):1–16.
[30] Qi N, Huang K, Fan Z, Xu B. Long-term energy management for microgrid with hybrid hydrogen-battery energy storage: a prediction-free coordinated optimization framework. Appl Energy 2025;377(PB):124485.
[31] Fang X, Wang Y, Dong W, Yang Q, Sun S. Optimal energy management of multiple electricity-hydrogen integrated charging stations. Energy 2023;262(PB):125624.
[32] Vivas FJ, Pajares A, Blasco X, Herrero JM, Segura F, Andújar JM. A novel energy management system based on two-level hierarchical economic model predictive control for use in microgrid control. Energy Convers Manage: X 2025;26(February):101027.
[33] Gondhalekar R, Ichi Imura J, Kashima K. Controlled invariant feasibility - a general approach to enforcing strong feasibility in MPC applied to move-blocking. Automatica 2009;45(12):2869–75.
[34] Son SH, Oh TH, Kim JW, Lee JM. Move blocked model predictive control with improved optimality using semi-explicit approach for applying time-varying blocking structure. J Process Control 2020;92:50–61.
[35] Kong Y, Xu N, Liu Q, Sui Y, Jia Y. Variable horizon-based predictive energy management strategy for plug-in hybrid electric vehicles and determination of a suitable predictive horizon. Energy 2024;294(October 2023):130809.
[36] Cao J, Peng J, He H. Research on model prediction energy management strategy with variable horizon. Energy Procedia 2017;105:3565–70.
[37] Gondhalekar R, Imurab JI. Least-restrictive move-blocking model predictive control. Automatica 2010;46(7):1234–40.
[38] Shekhar RC, Manzie C. Optimal move blocking strategies for model predictive control. Automatica 2015;61:27–34.
[39] Han K, Nguyen TW, Nam K. Battery energy management of autonomous electric vehicles using computationally inexpensive model predictive control. Electronics (Switzerland) 2020;9(8):1–19.
[40] Ma Y, Borrelli F, Hencey B, Packard A, Bortoff S. Model predictive control of thermal energy storage in building cooling systems. In: Proceedings of the IEEE Conference on Decision and Control; 2009. p. 392–7.
[41] Tatari FR, Banejad M, Kalat AA. A move blocking based direct voltage model predictive control to enhance the dynamic performance of DC microgrids containing constant power loads. IET Renew Power Gener 2023;17(13):3340–54.
[42] Rezayof Tatari F, Banejad M, Akbarzadeh Kalat A, Iwanski G. A long-horizon move-blocking based direct power model predictive control for dynamic enhancement of DC microgrids. Ain Shams Eng J 2024;15(7):102837.
[43] Shekhar RC, MacIejowski JM. Robust variable horizon MPC with move blocking. Syst Control Lett 2012;61(4):587–94.
[44] Schwickart T, Voos H, Darouach M, Bezzaoucha S. "A flexible move blocking strategy to speed up model-predictive control while retaining a high tracking performance. In: 2016 European Control Conference ECC; 2016. p. 764–9.
[45] Gondhalekar R, Imura J.I., Recursive feasibility guarantees in move-blocking MPC, Proceedings of the IEEE Conference on Decision and Control, no. Section IV. 2007; pp. 1374–1379.
[46] Wang T, Luo G, Liu C, Chen Z, Tu W. Speed control for variable speed PMSM drive system using nonlinear variable-horizon predictive functional control. IEEE J Emerg Selected Topics Power Electronics 2023;11(2):1454–65.
[47] Krishnamoorthy D, Biegler LT, Jäschke J. Adaptive horizon economic nonlinear model predictive control. J Process Control 2020;92:108–18.
[48] Choi Y, Lee W, Kim J, Yoo J. A variable-sampling time model predictive control algorithm for improving path-tracking performance of a vehicle. Sensors 2021;21(20).
[49] Persson L, Wahlberg B, Variable Prediction Horizon Control for Cooperative Landing on Moving Target In: IEEE Aerospace Conference Proceedings, 2021; vol. 2021-March.
[50] Hu Q, Amini MR, Kolmanovsky I, Sun J, Wiese A, Seeds JB. Multihorizon model predictive control: an application to integrated power and thermal management of connected hybrid electric vehicles. IEEE Trans Control Syst Technol 2022;30(3):1052–64.
[51] Hoffmann N, Andresen M, Fuchs FW, Asiminoaei L, Thogersen PB. Variable sampling time finite control-set model predictive current control for voltage source inverters. In: 2012 IEEE Energy Conversion Congress and Exposition ECCE; 2012. p. 2215–22.
[52] Vivas FJ, Segura F, Andújar JM, Calderón AJ, Isorna F. Battery-based storage systems in high voltage-DC bus microgrids. a real-time charging algorithm to improve the microgrid performance. J Storage Mater 2022;48(December 2021).
[53] Cagienard R, Grieder P, Kerrigan EC, Morari M. Move blocking strategies in receding horizon control. J Process Control 2007;17(6):563–70.
[54] Bustos R, Marín LG, Navas-Fonseca A, Reyes-Chamorro L, Sáez D. Hierarchical energy management system for multi-microgrid coordination with demand-side management. Appl Energy 2023;342(April):121145.
[55] Bordons C, Garcia-Torres F, Ridao M.A, Model Predictive Control of Microgrids. 2020.
[56] Zhu Y, Wang J, Bi K, Sun Q, Zong Y, Zong C. Energy optimal dispatch of the data center microgrid based on stochastic model predictive control. Front Energy Res 2022;10(March):1–9.
[57] Vivas Fernández FJ, Manzano FS, Márquez JMA, Calderón Godoy AJ. Extended model predictive controller to develop energy management systems in renewable source-based smart microgrids with hydrogen as backup. Theoretical foundation and case study. Sustainability (Switzerland) 2020;12(21):1–28.